ANALYSIS OF SHELL-TYPE STRUCTURES SUBJECTED TO TIME-DEPENDENT MECHANICAL AND THERMAL LOADING

A SEMI-ANNUAL STATUS REPORT
SUBMITTED TO
NASA-LEWIS RESEARCH CENTER
CLEVELAND, OHIO

By

G. J. Simitses and R. Riff

School of Aerospace Engineering
Georgia Institute of Technology
Atlanta, Georgia

April 1988

(NASA GRANT: NAG 3-534)

INTRODUCTION

The objective of the present research is to develop a general mathematical model and solution methodologies for analyzing structural response of thin, metallic shell-type structures under large transient, cyclic or static thermomechanical loads. Among the system responses, which are associated with these load conditions, are thermal buckling, creep buckling and ratcheting. Thus, geometric as well as material-type nonlinearities (of high order) can be anticipated and must be considered in the development of the mathematical model. Furthermore, this must also be accommodated in the solution procedures.

SUMMARY OF PROGRESS

The progress to date has been elaborated upon in an interim scientific report submitted to the sponsor during the summer of 1986, and in a series of semiannual progress reports. The most recent of these is dated October, 1987.

A complete true ab-inito rate theory of kinematics and kinetics for continuum and curved thin structures, without any restriction on the magnitude of the strains or the deformation, was formulated. The time dependence and large strain behavior are incorporated through the introduction of the time rates of the

metric and curvature in two coordinate systems; a fixed (spatial) one and a convected (material) coordinate system. The relations between the time derivative and the covariant derivatives (gradients) have been developed for curved space and motion, so that the velocity components supply the connection between the equations of motion and the time rate of change of the metric and curvature tenors.

The metric tensor (time rate of change) in the convected material coordinate system is linearly decomposed into elastic and plastic parts. In this formulation, a yield function is assumed, which is dependent on the rate of change of stress, metric, temperature, and a set of internal variables. Moreover, a hypoelastic law was chosen to describe the thermoelastic part of the deformation.

A time and temperature dependent viscoplastic model was formulated in this convected material system to account for finite strains and rotations. The history and temperature dependence were incorporated through the introduction of internal variables. The choice of these variables, as well as their evolution, was motivated by phenomenological thermodynamic considerations.

The nonisothermal elastic-viscoplastic deformation process was described completely by "thermodynamic state" equations. Most investigators (in the area of viscoplasticity) employ plastic strains as state variables. Our study shows that, in general,use of plastic strains as state variables may lead to inconsistencies with regard to thermodynamic considerations. Furthermore, the approach and formulation employed by all previous investigators lead to the condition that all plastic work is completely dissipated. This, however, is in contradiction with experimental evidence, from which it emerges that part of the plastic work is used for producing residual stresses in the lattice, which, when phenomenologically considered, causes hardening. Both limitations are not present in our formulation, because of the inclusion of the "thermodynamic state" equations.

The obtained complete rate field equations consist of the principles of the rate of the virtual power and the rate of conservation of energy, of the constitutive relations, and of boundary and initial conditions. These formulations provide a sound basis for the formulation of the adopted finite element solution procedures.

The derived shell theory, in the least restricted form, before any simplifying assumptions are imposed, has the following desirable features:

(a) The two-dimensional, impulse-integral form of the equations of motion and the Second Law of Thermodynamics (Clausius-Duhem inequality) for a shell follow naturally and exactly from their three-dimensional counterparts.
(b) Unique and concrete definitions of shell variables such as stress resultants and couples, rate of deformation, spin and

entropy resultants can be obtained in terms of weighted integrals of the three-dimensional quantities through the thickness.

(c) There are no series expansions in the thickness direction.

(d) There is no need for making use of the Kirchhoff Hypotheses in the kinematics.

(e) All approximations can be postponed until the descretization process of the integral forms of the First Law of Thermodynamics

(f) A by-product of the descent from three-dimensional theory is that the two-dimensional temperature field (that emerges) is not a through-the-thickness average, but a true point by point distribution. This is contrary to what one finds in the literature concerning thermal stresses in the shell.

To develop geometrically nonlinear, doubly curved finite shell elements the basic equations of nonlinear shell theories have to be transferred into the finite element model. As these equations in general are written in tensor notation, their implementation into the finite element matrix formulation requires considerable effort.

The nonlinear element matrices are directly derived from the incrementally formulated nonlinear shell equations, by using a tensor-oriented procedure. The classical thin shell theory based on the Kirchoff-Love hypotheses (Formulation D) was employed for this purpose. For this formulation, we are using the "natural" degrees of freedom per mid-surface shell node: three incremental velocities and the rates of rotations about the material coordinates in a mixed form.

A description of the developed element and related finite element code are given in Appendix A. This exposition provides information concerning the formulation, the finite element and how it is employed in the solution of shell-like configurations. A complete description including program flow chart, listing and instructions to the user is been finalized and it will be sent to the sponsor, separately.

The quasi-linear nature of the principle of the rate of virtual power suggests the adoption of an incremental approach to numerical integration with respect to time. The availability of the field formulation provides assurance of the completeness of the incremental equations and allows the use of any convenient procedure for spatial integration over the domain V. In the present instance, the choice has been made in favor of a simple first order expansion in time for the construction of incremental solutions from the results of finite element spatial integration of the governing equations.

The procedure employed permits the rates of the field formulation to be interpreted as increments in the numerical solution. This is particularly convenient for the construction of incremental boundary condition histories.

Even under the condition of static external loads and slowly growing creep effects, the presence of snap-through buckling makes the inertia effects significant. In dynamic analyses, the applied body forces include inertia forces. Assuming that the mass of the body considered is preserved, the mass matrix can be evaluated prior to the time integration using the initial configuration.

Finite element solution of any boundary-value problem involves the solution of the equilibrium equations (global) together with the constitutive equations (local). Both sets of equations are solved simultaneously in a step by step manner. The incremental form of the global and local equations can be achieved by taking the integration over the incremental time step $t=t_{j+1}-t_j$. The rectangular rule has been applied to execute the resulting time integration.

Clearly, the numerical solution involves iteration. A simplified version of the Riks-Wempner constant-arc-length method has been utilized. This iteration procedure which is a generalization of the displacement control method also allows to trace the nonlinear response beyond bifurcation points. In contrast to the conventional Newton-Raphson techniques, the iteration of the method takes place in the velocity and load rate space. The load step of the first solution in each increment is limited by controlling the length ds of the tangent. Either the length is kept constant in each step or it is adapted to the characteristics of the solution. In each step the triangular-size stiffness matrix has to be checked for negative diagonal terms, indicating that a critical point is reached.

One of the most challenging aspects of finite strain formulations is to locate analytical solution with which to compare the proposed formulation. Typically, as a first problem, a large strain uniaxial test case was analyzed. The case considered examines the rate-dependent plastic response of a bar to a deformation history that includes segments of loading, unloading, and reloading, each occurring at varying strain and temperature rates. Moreover, it was shown that the proposed formulation generates no strain energy under a pure rigid body rotation. These are surely important demonstration but they only represent a partial test because the principal stretch directions remain constant. Finally, a problem which was discussed by Nagtegaal and de Jong, and others too, as a problem which demonstrates limitations of the constitutive models in many strain formulation, is the Couette flow problem. This problem is solved as a third example. The results of these test problems show that:

- The formulation can accommodate very large strains and rotations.

- The formulation does not display the oscillatory behavior in the stresses of the Couette flow problem.

- The model incorporates the simplification associated with rate-insensitive elastic response without losing the ability to model rate temperature dependent yield strength and plasticity.

The problem of buckling of shallow arches under transient thermomechanical load was investigated next. The analysis was performed with the aid of 24 paralinear isoparametric elements. The paralinear isoparametric element is such that the thickness is small compared to other dimensions. The characteristics of the element are defined by the geometry and interpolation functions, which are linear in the thickness direction and parabolic in the longitudinal direction. Consequently, the element allows for shear strain energy since normals to a mid-surface before deformation remain straight, but not necessarily normal to the midsurface after deformation.

The developed solution scheme is capable of predicting response which includes pre- and post-buckling with thermal creep and plastic effects. The solution procedure was demonstrated through several examples which include both creep and snap-through behavior.

The last set of problems which are under investigation consists of creep or thermal buckling, with plastic effects, of shells of revolution.

In addition, following a more traditional approach, a method was developed for bounding the response (solution) of bars and beams of (linear) viscoelastic material behavior, based on nonlinear kinematic relations.

In connection with this progress to date, two papers were published by the AIAA Journal in 1986. Moreover, a paper entitled, "Non-Isothermal Elastoviscoplastic Analysis of Planar Curved Beams" was presented at the 3rd Symposium on Nonlinear Constitutive Relations for High-Temperature Applications, held at the University of Akron, on June 11-13, 1986. A descriptive abstract of this paper was published in the meeting proceedings and the full paper will appear in a special publication. Copies of the above have been sent to the sponsor.

In addition, the two papers presented at the 28th AIAA/-ASME/ASCE/AHS SDM Conference and published in the proceedings of this conference, and the one paper presented at the 21st Conference of the Israel Society of Mechanical Engineers (keynote lecture by Dr. R. Riff) been accepted for publication; the first two by the AIAA Journal and the last one by the International Journal of Computers and Structures. These three papers deal with applications to snap-through and creep buckling of bars and arches, and to two-dimensional problems in extension and shear. Most of this work was also presented at the NASA-Lewis Conference on Structural Integrity and Durability of Reusable Space Prop-

ulsion Systems on May 1987 in Cleveland. Copies of these papers have been sent to the Sponsor.

In connection with the more traditional approach a paper accepted for presentation and for publication in the Proceedings of the special Symposium on Constitutive Equations at the ASME Winter Annual Meeting, Chicago, IL., November 28 - December 2, 1988. The title of the paper is "Creep Analysis of Beams and Arches Based on a Hereditary Visco- Elastic- Plastic Constitutive Law" and a copy of the paper is attached herewith.

Moreover, two papers are presently in preparation, and will be submitted for publication during the month of May. One deals with applications to shell configurations, and it is titled "Analysis of Shell Structures Subjected to Large Mechanical and Thermal Loadings". The second deals with the time- dependent response of curved structural elements, and it is titled "The Dynamic Aspects of Thermo- Elasto- Viscoplastic Snap- Through and Creep Phenomena". Copies of these papers will be sent to the sponsor with the next semi- annual report.

The study was initially limited only to the simplest of the developed shell theory formulations (Formulation D).

The various shell theory approximations (formulations) are based on the use of certain simplifying assumptions regarding the geometry and kinematics of the shell configuration.

These are:

Assumption I: The material points which are on the normal to the reference surface before deformation will be on the same normal after deformation.
Assumption II: The shell is sufficiently thin so that we can assume linear dependence of the position of any material point (in the deformed state) to the normal (to the reference surface) coordinate (in the deformed state). The linear dependence can easily be changed to parabolic, cubic, or any desired degree of approximation.
Assumption III: The rate of change of the velocity gradients with respect to in-plan coordinates on the two bounding shell surfaces is negligibly small.
Assumption IV: The rate of change of the distance of a material from the reference surface is negligibly small.

On the basis of the above four simplifying assumptions, several formulations result, for the analysis of thin shells. These formulations are denoted below by capital letters.

Formulation A: This formulation makes use of Assumption I,only.
Formulation B: This formulation employs Assumptions I and II.
Formulation C: This formulation employs Assumption I, II and

III.

Formulation D: This is the classical thin shell theory based on the Kirchhoff-Love hypotheses of Assumptions I, II, III, IV, as applied to large deformation theory.

These formulation are arranged in such a manner that we move from the least restrictive (A) to the most restrictive (D).

In addition to this a fifth formulation (E) can easily be devised and this formulation in terms of order of restriction is similar to Formulation A. Formulation E makes use of Assumption II only.

FUTURE TASKS

The main thrust of the additional tasks is to develop a finite element and select a code, which will be made available to all users and which will be based on the most general (but practical) nonlinear shell formulation possible and nonlinear constitutive relations to predict the response of shell-like structures, when subjected to time-dependent thermomechanical loads with large excursions.

In order to accomplish the overall objective, as stated a number of steps or tasks need be completed. These are:

Step 1: Formulation the principle of the rate of virtual power for the less restricted shell formulation (C, B, E, A).

Step 2: Couple the general constitutive relations to shell kinematics for the aforementioned formulations.

Step 3: Before developing a finite element, and before numerically testing and comparing the merits of the various formulations, some theoretical evaluation of the degree of approximation will be attempted.

Step 4: Develop a finite element for the chosen least restrictive shell formulation. In order to accomplish this some novel ideas and procedures will be employed. These include a tensor-oriented procedure for obtaining the element, and a discretization process that involves not only the nodal degrees of freedom but also an approximation to the "shift" tensors.

Step 5: Incorporate the developed finite element and related constitutive relations into a FEM code.

Step 6: Numerically test and evaluate the developed finite element procedure.

It is estimated that this entire research effort will require a minimum of three years to bring to fruition. Some of the tasks (steps 1 and 2) have already been started.

APPENDIX A - THE SHELL ELEMENT

A brief description highlighting the essential features of the shell element development and the related code used in this work is given here.

In order to derive discrete algorithm based on the finite element displacement method we approximate the velocity field by index-oriented notation, which allows the separate representation of the shape functions (the specific expression depends on the decided upon degress - of - freedom, Lagrangian, Hermitian, etc.) for the tangential velocities v_α and for the normal velocity v_3 .

$$v_\alpha = v_\alpha^M V_M = V^M v_{\alpha M} \tag{1}$$

$$v_3 = v_3^M V_M = V^M v_{3M} \tag{2}$$

Upper indices imply the columns, lower indices the rows of a matrix expression, and the summation is carried out spanning the number of degrees-of-freedom. V^M and V_M represent, therefore, the vector of nodal velocities by the row and by the column respectively. We get the shape functions for the partial derivatives of the velocity shape functions v_α^M , v_3^M :

$$v_{\alpha,\beta} = \left(v_\alpha^M\right)_{,\beta} V_M = v_{\alpha,\beta}^M V_M \tag{3}$$

$$v_{3,\beta} = \left(v_3^M\right)_{,\beta} V_M = v_{3,\beta}^M V_M \tag{4}$$

The main idea of this formulation is the development of shape functions for further mechanical and thermal variables by the application of well-known tensor procedure on the basic shape functions (3) and (4). Taking, for example, the covariant derivative

$$v_{\alpha;\beta} = v_{\alpha,\beta} - v_\lambda \Gamma_{\alpha\beta}^\lambda \tag{5}$$

and inserting (3) and (1), we can define the shape function of the covariant derivative:

$$v_{\alpha;\beta} = \underbrace{\left(v_{\alpha,\beta}^M - v_\lambda^M \Gamma_{\alpha\beta}^\lambda\right)}_{v_{\alpha;\beta}^M} V_M = v_{\alpha;\beta}^M V_M \tag{6}$$

In the same way we receive the shape function of the internal variables, for example the rate of deformation and the spin tensors:

$$d_{(\alpha\beta)} = \frac{1}{2}\left(v_{\alpha;\beta} + v_{\beta;\alpha} - 2 b_{\alpha\beta} v_3\right) =$$

$$\underbrace{\frac{1}{2}\left(v_{\alpha;\beta}^M + v_{\beta;\alpha}^M - 2 b_{\alpha\beta} v_3^M\right)}_{d_{(\alpha\beta)}^M} V_M = d_{(\alpha\beta)}^M V_M \tag{7}$$

$$w_{(\alpha\beta)} = -\left(v_{3;\alpha\beta} + v_{\lambda;\alpha}\, b^{\lambda}_{\beta} + v_{\lambda;\beta}\, b^{\lambda}_{\alpha} + v_{\lambda}\, b^{\lambda}_{\alpha;\beta} - v_{3}\, b_{\lambda\alpha}\, b^{\lambda}_{\beta}\right) =$$

$$-\underbrace{\left(v^{M}_{3;\alpha\beta} + v^{M}_{\lambda;\alpha}\, b^{\lambda}_{\beta} + v^{M}_{\lambda;\beta}\, b^{\lambda}_{\alpha} + v^{M}_{\lambda}\, b^{\lambda}_{\alpha;\beta} - v^{M}_{3}\, b_{\lambda\alpha}\, b^{\lambda}_{\beta}\right)}_{w^{M}_{(\alpha\beta)}} V_M = \tag{8}$$

$$= w^{M}_{(\alpha\beta)}\, V_M$$

The same procedure is now applied to the shift tensor

$$M^{-1}{}^{\wedge}_{\tau} = \left(\delta^{\gamma}_{\beta} + \zeta_0\, b^{\gamma}_{\beta}\right) \delta^{\beta}_{\tau}\, \delta^{\wedge}_{\gamma} + \delta^{3}_{\tau}\, \delta^{M}_{3} \tag{9}$$

which is responsible for the "exact" distributions over the thickness.

Finally the shape functions of the internal forces and temperature variables can be derived from the shape functions of the rate of deformation and spin tensor via the constitutive relations; for example:

$$N^{(\alpha\beta)} = \underbrace{D H^{\alpha\beta\rho\tau}\, v^{M}_{(\rho\tau)}}_{N^{(\alpha\beta)M}}\, V_M = N^{(\alpha\beta)M}\, V_M \tag{10}$$

All these expression are now substituted into the rate of the first law of thermodynamics to obtain the element "stiffness" equations. The developed element matrices are implemented into the global relation of the complete shell structure by standard assemblage process considering incidence and boundary conditions.

The present curvilinear formulation of the element enables the precise description of geometry, external loads and temperatures and the fulfillment of the convergence criteria, while the rigid body motion condition can only be satisfied in an approximate manner. The tensor oriented formulation renders the optional use of various shape functions for the tangential velocities v and the normal velocity v_3.

The shell element which have been used up to today is based on the bicubic Hermite polynomial with 4x12 generalized velocities and 4 temperatures. Numerical integration spanning the element domain was applied (16 points of integration), whereby area and boundary integrals were replaced by double integration with respect to the curvilinear θ^{α} - coordinates.

$$dA = \sqrt{(a)}\; d\theta^{1}\, d\theta^{2} \tag{11}$$

$$dS = \sqrt{(a_{\alpha\beta}\, d\theta^{\alpha}\, d\theta^{\beta})} \tag{12}$$

FLOW CHART FOR THE SET-UP OF THE ELEMENT MATRICES

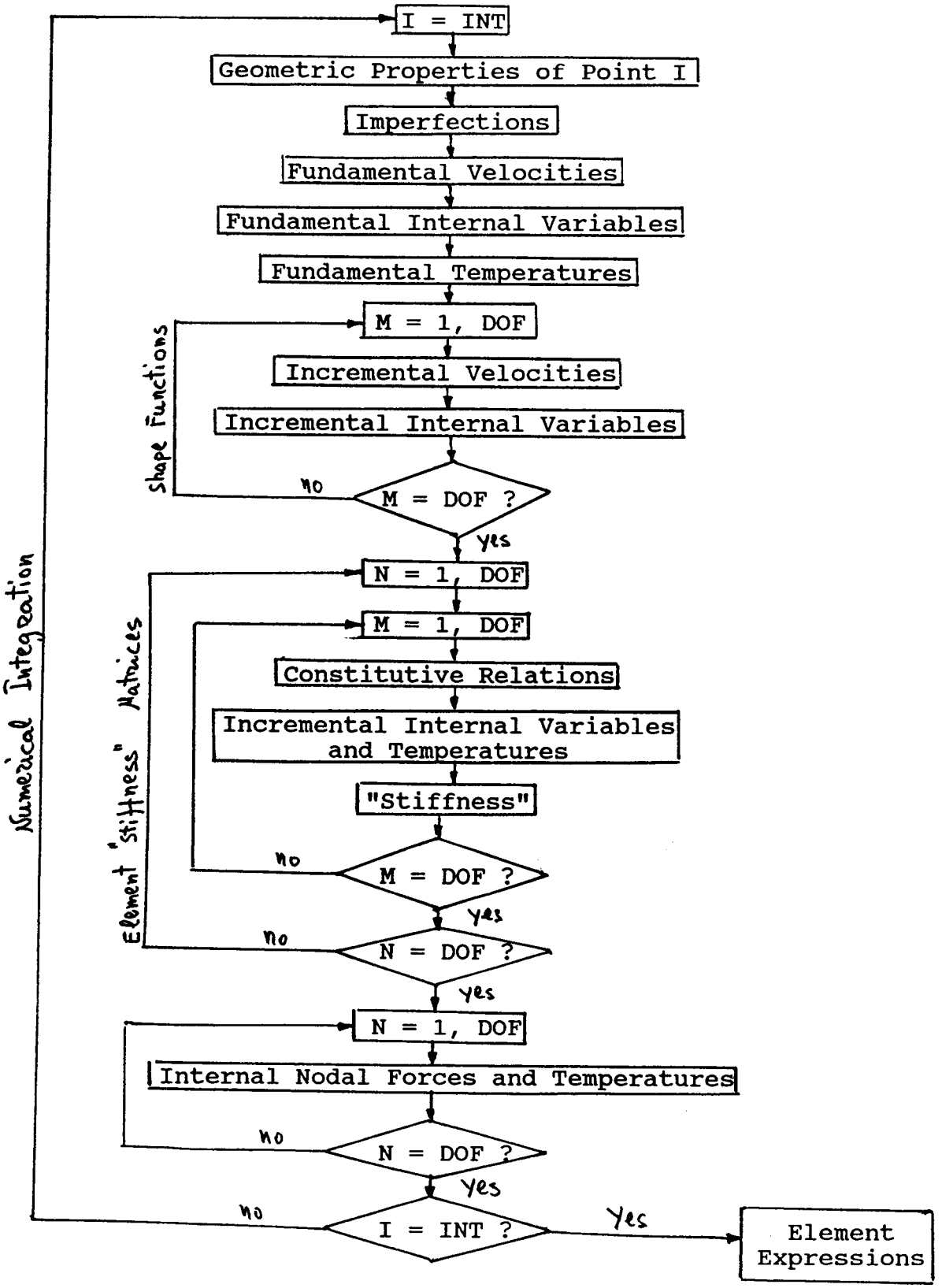

CREEP ANALYSIS OF BEAMS AND ARCHES BASED ON A HEREDITARY VISCO-ELASTIC-PLASTIC CONSTITUTIVE LAW

by

John M. Stubstad* and George J. Simitses**
Georgia Institute of Technology
Atlanta, Georgia

ABSTRACT

In both the nuclear power and aerospace industries, it is not uncommon to find metallic structural elements which are subjected to significant thermal excursions from an elevated ambient temperature. Depending upon the nominal ambient temperature and the magnitude of the thermal cycle, this can cause the time-dependent properties of the material to change radically during each duty cycle. At the lower temperatures of the duty cycle, the material may behave primarily in a viscoelastic manner. However, as the temperature or mechanical loading increases, plastic-type behavior may predominate. These modifications of the behavior of the material substantially complicate the analysis of the problem, thereby making prediction of the ultimate useful life of such an element exceedingly difficult.

The paper presents an analytic study of planar beams and arches subjected to significant thermal cycling from ambient temperatures up to 800°C. In the study, a recently developed unified nonlinear hereditary type of viscoelastoplastic constitutive law is employed to characterize the time- and temperature-dependent properties of a typical aerospace alloy, Hastelloy X.

The results from this work demonstrate that a strong interaction exists between the back stress variable of this particular constitutive law and the time-dependent stress distribution produced by the geometry of the deformation. Effectively, this interaction tends to control, in a highly nonlinear manner, the creep-ratchetting response of the beam and the arch. An unexpected consequence of this is that temperature gradients in the thickness direction, a factor normally neglected in most studies, tends to exert an important influence on the response during thermal cycling.

NOMENCLATURE

a	load eccentricity
A	cross sectional area of beam or arch
b	width of beam or arch
c_{ij}	inelastic strain tensor
d	deformation vector for points on the centroidal axis
E	Young's Modulus
E_0, E_1, and E_2	zero, first and second moments of the elastic modulus across a cross section, respectively

* currently with the Aerospace Corporation; Member of ASME

** Professor of Aerospace Engineering; Member of ASME

$\mathbf{g}_\alpha$, $\mathbf{G}_\alpha$	base vectors for undeformed and deformed configurations, respectively
$g_{\alpha\beta}$ $G_{\alpha\beta}$	metric components of the undeformed and deformed configurations, respectively
h	depth of beam or arch
k	$\kappa + \frac{\partial \phi}{\partial s}$
K	drag stress
K_1 , K_2 , n_1 thru n_7	constitutive law constants
m and n	constitutive law exponents
M and N	moment and force resultants, respectively
M_c and N_c	creep strain moment and force pseudo-resultants, respectively
M_θ and N_θ	thermal strain moment and force pseudo-resultants, respectively
p	pressure load
P and V	axial and transverse force resultants acting on the cross section
$Q(t)$ and $\Upsilon(t)$	constitutive law functions
r and R	position vectors in undeformed and deformed configurations, respectively
s and η	coordinates along length and depth directions, respectively
s_{ij}	components of the deviator stress tensor
t, n and k	triad of unit vectors for the undeformed configuration
T, N and K	triad of unit vectors for the deformed configuration
t	time
u and w	axial and transverse displacement of the centroidal axis, respectively
α	coefficient of thermal expansion
ϵ_o	centroidal axis strain
ϵ_{ij}	strain tensor component
Θ	change in temperature
κ	initial curvature of the arch
λ and μ	Lamè constants
σ_{ij}	stress tensor component
ϕ	angle of rotation of cross section
Ω_{ij}	backstress

INTRODUCTION

It is well known that metal alloys can undergo transitions in behavior as temperature increases. Commonly, for loading substantially below yield, the elastic response observed at room temperature generally gives way to a time-dependent viscoelastic response at somewhat elevated temperatures. Further increases in temperature, however, introduces the potential for sudden "rapid" or plastic type deformation. Such transitions create the potential for significantly shortening the useful life of the structural element and ultimately generate the possibility for a sudden unanticipated failure. Consequently, for many years the aerospace and nuclear power industries, where elevated temperature operating environ-

ments abound, have had a continuing interest in predicting the behavior of metallic structural elements subjected to such conditions.

Early investigators, such as Hilton and others [1–3], generally focused their attention on the behavior of structural components subjected to conditions of constant load at constant uniform elevated temperatures. Many of these studies employed simplified analyses to improve mathematical tractability. Additionally, "experimentally based equation of state" type constitutive laws were often used to express the nonlinear elevated temperature time-dependent behavior of the material. A summary of many of methods developed and key findings obtained from these studies is available in Hoff [4].

These efforts provided answers to many of the questions regarding elevated temperature creep buckling. However, they were not able to satisfactorily describe the creep ratchetting behavior resulting from elevated temperature thermal cycling. Consequently, it was not until the efforts of Miller [5] and Edmunds and Beer [6], both of whom considered nuclear pressure vessels, that this particular form of behavior was specifically addressed. Subsequently, Bree [7,8] investigated the basic factors which determine when this type of response could occur. Of course, these early studies lead to many subsequent efforts which explored various aspects of the phenomena. Some of these studies relied on experimental investigations while others employed analytic approaches. In this regard, the works of Conway et. al. [9], Corum [10,11] and Mukhejeree, Kumar and Chang [12] provide a representative sampling of the types of studies which were conducted.

However, the greatest concentration of effort related to this topic area has been the associated effort directed toward improving the capability to predict the elevated temperature behavior of metals. The contributions of Hart [13,14], Pointer and Leckie [15], Pugh [16–18], Krempl [19], and Walker and Krempl [20], to name of few, provide a dramatic illustration of the intensity of these efforts to develop and employ advanced constitutive models. Yet, as pointed out by Corum and Sartory [21], an equation of state approach to constitutive modeling is still generally used in design situations. However, as Pugh [18] has noted, the newer types of unified constitutive laws, where inelastic strain is not divided into distinct creep and plasticity components, can provide an alternate approach.

Consequently, one of the aims of this study is to examine the use of a typical unified constitutive model in an analysis of the behavior of structural elements subject to thermal cycling from an elevated ambient temperature. The specific law which was selected is one developed by Walker [22] to model the time- and temperature-dependent behavior of Hastelloy X, an alloy routinely used in the aeropsace industry.

The results of this study indicate that, for this particular form of constitutive law, an implicit interaction exists between the actual stress in the member and the backstress variable of the constitutive law. This interaction is shown to strongly influence the ultimate response of the element. This result is significant for two reasons. First, because saturation of the backstress of this constitutive law can lead to plastic response, which signifies that the ultimate reliability of any predicted results rests strongly upon the accuracy with which the backstress growth law parameters have been determined.

Additionally, this particular aspect produces the rather interesting result that, due to the strong temperature dependence of the material constants of the law, temperature variations in the thickness direction greatly influence predicted response. This is a significant for any analysis since the influences

of such temperature variations are generally neglected in most studies.

MATHEMATICAL FORMULATION

To focus principally upon the interaction between the response of the structural element and the prediction of thermal dependence of the material, the problem is formulated within the context of a simplified beam theory. Consequently, it is assumed that the beam or arch deforms in accordance with the Euler-Bernoulli hypotheses. As such, cross sectional planes normal to the centroidal axis in the undeformed geometry are assumed to remain plane and normal in the deformed state. Similarly, extensional straining in the thickness and depth directions are neglected. Therefore, based on the geometry illustrated in Fig. 1, the position vectors $\mathbf{r}$ and $\mathbf{R}$, where

$$\mathbf{r} = \mathbf{r}_o + \eta\mathbf{n} \quad \text{and} \quad \mathbf{R} = \mathbf{r}_o + \mathbf{d} + \eta\mathbf{N} \tag{1}$$

are employed to locate a typical point on an arbitrary cross section in the undeformed and deformed configurations, respectively. Note that η represents the coordinate in the normal direction. Also, lower case and upper case symbols are employed to denote quantities referred to the undeformed and deformed configurations, respectively.

Base vectors for the reference and current state, $\mathbf{g}_\alpha$ and $\mathbf{G}_\alpha$, respectively, are defined by

$$\mathbf{g}_\alpha = \frac{\partial \mathbf{r}}{\partial \alpha} \quad \text{and} \quad \mathbf{G}_\alpha = \frac{\partial \mathbf{R}}{\partial \alpha} \qquad \text{where} \quad \alpha = s, \eta \tag{2}$$

Consequently, the deformation vector which translates a typical point from the undeformed to deformed configurations, denoted as $\mathbf{d}$, can be expressed as

$$\mathbf{d} + \bar{\eta}\mathbf{N} = (u + \eta \sin\phi)\mathbf{t} + (w + \eta\cos\phi)\mathbf{n} \tag{3}$$

where u and w represent axial and transverse displacement functions for points on the centroidal axis, respectively. Thus, upon substituting Eqns. (1) and (3) into (2), differentiating and employing the Fernet-Serret formulae and the strain definition,

$$\gamma_{\alpha\beta} = \frac{1}{2}(G_{\alpha\beta} - g_{\alpha\beta}); \qquad \text{where} \quad g_{\alpha\beta} = \mathbf{g}_\alpha \cdot \mathbf{g}_\beta \,, \quad G_{\alpha\beta} = \mathbf{G}_\alpha \cdot \mathbf{G}_\beta \tag{4}$$

yields the strain expressions

$$\gamma_{ss} = \frac{1}{2}\{(1 + \frac{\partial u}{\partial s} + \kappa w + \eta k\cos\phi)^2 + (\frac{\partial w}{\partial s} - \kappa u - \eta k \sin\phi)^2 - (1 + \eta\kappa)^2\} \tag{5a}$$

$$\gamma_{s\eta} = \gamma_{\eta s} = \frac{1}{2}\{(1 + \frac{\partial u}{\partial s} + \kappa w + \eta k\cos\phi)\sin\phi + (\frac{\partial w}{\partial s} - \kappa u - \eta k\sin\phi)\cos\phi\} \tag{5b}$$

and

$$\gamma_{\eta\eta} = \frac{1}{2}\{\sin^2\phi + \cos^2\phi - 1\} = 0 \tag{5c}$$

Note that in these expressions, $k = \kappa + \partial\phi/\partial s$, where κ denotes the initial constant curvature of the arch and ϕ represents the angle of rotation of the cross section.

From the Euler-Bernoulli hypotheses, the shear strains must vanish. Consequently, from this requirement Eqn. (5b) yields

$$\tan\phi = \frac{-\left(\frac{\partial w}{\partial s} - \kappa u\right)}{\left(1 + \frac{\partial u}{\partial s} + \kappa w\right)} \tag{6}$$

Therefore, employing the definition

$$1 + 2\epsilon_o = \left(1 + \frac{\partial u}{\partial s} + \kappa w\right)^2 + \left(\frac{\partial w}{\partial s} - \kappa u\right)^2 \tag{7}$$

and Eqn. (6) it is relatively easy to show that

$$\sin\phi = \frac{-\left(\frac{\partial w}{\partial s} - \kappa u\right)}{\sqrt{1 + 2\epsilon_o}} \quad \text{and} \quad \cos\phi = \frac{1 + \frac{\partial u}{\partial s} + \kappa w}{\sqrt{1 + 2\epsilon_o}} \tag{8}$$

Thus, expanding Eqn. (5a) and employing Eqns. (7) and (8) yields

$$\gamma_{ss} = \epsilon_o + \eta\left\{\kappa\sqrt{1 + 2\epsilon_o} - \kappa + \sqrt{1 + 2\epsilon_o}\frac{\partial\phi}{\partial s}\right\} + \eta^2\left\{\kappa + \frac{1}{2}\frac{\partial\phi}{\partial s}\right\}\frac{\partial\phi}{\partial s} \tag{9}$$

From the above it is clear that ϵ_o represents the strain induced along the centroidal axis. Since, for a thin arch or beam, the last term of Eqn. (9) should be small in comparison to the others, it may be neglected. Similarly, additional simplifications may be obtained for the case where the centroidal axis strain is sufficiently small so that it may be neglected in comparison to one. Based on these assumptions, Eqn. (9) simplifies to the standard form

$$\gamma_{ss} \approx \epsilon_o + \eta\frac{\partial\phi}{\partial s} \tag{10}$$

Equilibrium equations are obtained through application of the Principle of Virtual Work. Stress resultants, N and M, are defined such that

$$\mathrm{N} = \int_A \sigma\, dA \quad \text{and} \quad \mathrm{M} = \int_A \sigma\eta\, dA \tag{11}$$

Employing the deformed configuration geometry illustrated in Fig. 2, it is noted that

$$\delta\phi = \frac{\partial\delta v_1}{\partial s} + k\delta v_2 \tag{12a}$$

$$\delta\epsilon = \frac{\partial\delta v_2}{\partial s} - k\delta v_1 \tag{12b}$$

where $\delta\phi$ and $\delta\epsilon$ denote the incremental increases in rotation and centroidal axis strain resulting from the deformed configuration axial and transverse displacements, v_1 and v_2, respectively.

Consequently, from the Principle of Virtual Work,

$$\delta W_{ext} = [\mathrm{M}\delta\phi + \mathrm{N}\delta v_1 + \mathrm{Q}\delta v_2]_1^2 + \int_1^2 -p^*\delta v_2\, ds \tag{13}$$

Expressing the first term on the right hand side in terms of an integral over the length and then combining that result with the work term yields

$$\delta W_{ext} = \int_1^2 \left[\frac{\partial \mathrm{M}}{\partial s}\delta\phi + \mathrm{M}\frac{\partial \delta\phi}{\partial s} + \frac{\partial \mathrm{N}}{\partial s}\delta v_1 + \mathrm{N}\frac{\partial \delta v_1}{\partial s} + \frac{\partial \mathrm{Q}}{\partial s}\delta v_2 + \mathrm{Q}\frac{\partial \delta v_2}{\partial s} - p^*\delta v_2 \right] ds \tag{14}$$

Therefore, employing Eqns. (12) and noting that terms multiplying the virtual displacements δv_1, δv_2 and $\delta\phi$ must vanish identically yields, after eliminating the shear resultant, the equilibrium equations

$$k\mathrm{N} - \frac{\partial^2 \mathrm{M}}{\partial s^2} = p^* \quad \text{and} \quad \frac{\partial \mathrm{N}}{\partial s} + k\frac{\partial \mathrm{M}}{\partial s} = 0 \tag{15}$$

with the associated boundary conditions at $s = 0,\ l$

$$\begin{aligned} \mathrm{N} = \mathrm{N}^* \quad &\text{or} \quad \delta v_1 = 0 \\ \frac{\partial \mathrm{M}}{\partial s} = -\mathrm{Q}^* \quad &\text{or} \quad \delta v_2 = 0 \end{aligned} \tag{16}$$

and

$$\mathrm{M} = \mathrm{M}^* \quad \text{or} \quad \delta\phi = 0$$

where N^*, Q^*, and M^* denote the axial, shear and moment resultants applied at the ends of the arch, respectively.

Expressions for the force and moment resultants, N and M, respectively, are obtained from the constitutive law. A unified hereditary visco-elastic-plastic law developed by Walker [22] to characterize the time and temperature dependence of Hastelloy X is employed in this study. The selection of Walker's functional theory, a highly generalized representation for a three parameter viscoelastic solid, was based principally upon three considerations. First, from a strictly practical point of view, a substantial body of experimental work [22–24] had been performed to establish the temperature dependence of the constitutive law parameters for a wide range of temperatures. These efforts included a validation which examined the predictive capability of the law through a comparison of analytical and experimental results for time variable thermo-mechanical load cycling of uniaxial specimens.

A second factor which favored selection of the Walker law was that the law is able to reproduce certain forms of classical behavior as a limiting case. For example, saturation of the drag stress parameter produces an effect equivalent to isotropic hardening of a material. Similarly, saturation of the backstress produces an effect equivalent to kinematic hardening. Finally, the associated laws which govern the evolution of the state variables provide for the opportunity to include effects related to both dynamic and static thermal recovery.

The final reason for selection of the Walker law is that it can be expressed in both differential and integral formats. For this particular study, the differential format of the law was found to be the most convenient. However, it was hope that the availability of an integral format would provide, at a future date, the opportunity to extend some prior work involving kinematic bounding of nonlinear integral formulations [25] to also include some form of constitutive bounding.

The general integral form of Walker's functional theory has been provided in Appendix A. That appendix also contains a derivation of the differential form from the integral format. It should be noted

that, in the modeling of the elevated temperature behavior of Hastelloy X, additional simplifications in the form of the law were possible . These simplifications resulted from the fact that, for Hastelloy X, a number of material constants are zero over the entire temperature range.

As a result of these various simplifications, the differential format of Walker's functional theory, for one-dimensional loading of Hastelloy X, has the general form

$$\dot{\epsilon_c} = \text{sign}(\sigma - \Omega_{11})\Big(\frac{\text{abs}(\sigma - \Omega_{11})}{K}\Big)^n \tag{17a}$$

$$\dot{\Omega}_{11} = \dot{\Omega}^o_{11} + n_2\dot{\epsilon_c} - (\Omega_{11} - \Omega^o_{11})(\dot{G} - \frac{1}{n_2}\frac{\partial n_2}{\partial \Theta}\dot{\Theta}) \tag{17b}$$

$$\dot{\Omega}^o_{11} = \frac{\Omega^o_{11}}{\Omega^o}\dot{\Theta} \tag{17c}$$

$$K = K_1 \tag{17d}$$

and

$$\dot{G} = n_3\,\text{abs}(\dot{\epsilon_c}) + n_\theta\big(\text{abs}\{\Omega_{11}\}\big)^{m-1} \tag{17e}$$

Finally, since the time rate of change of temperature is relatively low in the sample problems, all terms where $\dot{\Theta}$ appeared were assumed to be insignificant and therefore neglected. Note that this provides some minor simplifications to Eqn. (17b) and makes the reference backstress, Ω^o_{11}, independent of the time rate of change in temperature.

The law is postulated upon an additive decompostion of the total strain into elastic, thermal and inelastic components, ϵ_e, ϵ_θ and ϵ_c, respectively. Therefore

$$\epsilon_o + \eta\frac{\partial \phi}{\partial s} = \epsilon_e + \epsilon_\theta + \epsilon_c \tag{18}$$

Thus, for the state of one-dimensional loading considered in this study, this yields

$$\sigma = E(\epsilon_o + \eta\frac{\partial \phi}{\partial s} - \epsilon_\theta + \epsilon_c) \tag{19}$$

Therefore, integrating this expression over the cross section and employing the force resultant definition, Eqn. (11), yields

$$\mathrm{N} = E_0\epsilon_o + E_1\frac{\partial \phi}{\partial s} - \mathrm{N}_\theta - \mathrm{N}_c \tag{20}$$

where E_0 and E_1 denote the zero and first integrals of the elastic modulus over the cross section and N_θ and N_c represent "pseudo-resultant" type quantities defined as

$$\mathrm{N}_\theta = \int_A E\epsilon_\theta\, dA \quad \text{and} \quad \mathrm{N}_c = \int_A E\epsilon_c\, dA \tag{21}$$

Note that the first integral of the elastic modulus over the cross section, E_1, does not necessarily vanish since it is presumed that the elastic modulus can be a function of temperature which is not necessarily

constant across a cross section. An interseting aspect of this is that it induces a form of bending-stretching coupling { see also Eqn. (22) } similar to that of which can occur in a laminated composite material. Finally, it should be noted that, although the quantities defined by Eqn. (21) each have the units of a force resultant, these definitions are merely employed as a mathematical convenience to simplify subsequent expressions.

Multiplying Eqn. (19) by the thickness coordinate, η, integrating over the cross section and employing the moment resultant definition, Eqn. (12), similarly yields

$$\mathrm{M} = E_1\epsilon_o + E_2\frac{\partial\phi}{\partial s} - \mathrm{M}_\theta - \mathrm{M}_c \tag{22}$$

where E_2 denotes the second integral of the elastic modulus over the cross section and the "pseudo-moment" resultants are defined by

$$\mathrm{M}_\theta = \int_A \eta E\epsilon_\theta\, dA \quad \text{and} \quad \mathrm{N}_c = \int_A \eta E\epsilon_c\, dA \tag{21}$$

Consequently, substituting Eqns. (20) and (22) into Eqns. (15) yields the general governing relations

$$kE_0\epsilon_o + kE_1\frac{\partial\phi}{\partial s} - E_1\frac{\partial^2\epsilon_o}{\partial s^2} - E_2\frac{\partial^3\epsilon_o}{\partial s^3} = p^* + k(\mathrm{N}_c + \mathrm{N}_\theta) + \frac{\partial^2}{\partial s^2}(\mathrm{M}_c + \mathrm{M}_\theta) \tag{22}$$

and

$$(E_0 + kE_1)\frac{\partial\epsilon_o}{\partial s} + (E_1 + kE_2)\frac{\partial^2\phi}{\partial s^2} = \frac{\partial}{\partial s}(\mathrm{N}_c + \mathrm{N}_\theta) + k(\mathrm{M}_c + \mathrm{M}_\theta) \tag{23}$$

Note that, in the development of these relationships, it is assumed that the moments of the elastic modulus, E_0, E_1 and E_2 are constant with respect to the axial coordinate. This implies that these quantities are independent of stress or strain and also that the temperature is constant along the length direction.

Equations (22) and (23) represent a pair of interrelated spatially dependent nonlinear differential relationships which describe the deformation of the beam or arch. In their present form, they are stated in terms of the strain along the centroidal axis and the rotation of the cross section. These two quantities, in turn, are interrelated through the axial and transverse displacements of the centroidal axis. Substitution of the appropriate expressions for the centroidal axis strain and cross section rotation ultimately results in a set of equations, one of third order and the other of fourth order, in terms of these displacement functions.

Due to the significant nonlinearity of these equations, a numerical method of solution was selected. The particular method employed is an adaptation of Newton's method for the solution of nonlinear algebraic equations [26]. The basic approach is to develop an iterative procedure in which a "close" trial solution can be directed towards the actual solution. Note that this method neither guarantees convergence to a solution nor that any solution found is unique.

The basic methodology is to expand a nonlinear differential term such as $\mathrm{dX}^m\mathrm{dY}^n$, where dX and dY represent differentials of the functions X and Y and m and n represent integer exponents, into the sum and products of trial solutions $\bar{\mathrm{X}}$ and $\bar{\mathrm{Y}}$ and corrections of the form $\Delta\mathrm{X}$ and $\Delta\mathrm{Y}$. Consequently, substituting $\mathrm{X} = \bar{\mathrm{X}} + \Delta\mathrm{X}$ and $\mathrm{Y} = \bar{\mathrm{Y}} + \Delta\mathrm{Y}$ yields,

$$dX^m dY^n = d\bar{X}^m\, d\bar{Y}^n + m d\bar{X}^{m-1}\, d\bar{Y}^n d(\Delta X) + n d\bar{X}^m\, d\bar{Y}^{n-1} d(\Delta Y) + f(\bar{X}, \bar{Y}) O[\Delta X, \Delta Y] \tag{24}$$

where $f(\bar{X}, \bar{Y})O[\Delta X, \Delta Y]$ represents a nonlinear function of $\bar{X}$ and $\bar{Y}$ of second and higher order terms in ΔX and ΔY. Provided the trial solution is close to the true solution, these higher order terms should be small in comparison to the linear terms and thus may be neglected. Consequently, the nonlinear term may be closely approximated by the linear form

$$dX^m dY^n \approx d\bar{X}^m\, d\bar{Y}^n + m d\bar{X}^{m-1}\, d\bar{Y}^n d(\Delta X) + n d\bar{X}^m\, d\bar{Y}^{n-1} d(\Delta Y) \tag{25}$$

By employing the technique described above, the nonlinear differential terms appearing in the governing equations are approximated in terms of linear differential equations for the corrections to assumed trial functions. These coupled differential equations are then converted to a set of coupled algebraic relations through the approximation of the linear derivative terms for the corrections to the assumed deflections using central difference formulae. Appendix B provides, for example, the general finite difference expressions developed for the initially circular arch.

A matrix iteration procedure is employed to refine an assumed trial solution. Each sucessive set of corrections is used to update the trial solution until convergence is obtained. Tests for such convergence included the consideration of the magnitude of each set of corrections as well as the overall accuracy for which each of the individual nodal equations was solved. In this regard it is noted that an equivalent degree of coupling did not exist between the in-plane and transverse equations of equilibrium. Typically, the accuracy of the solution of the transverse equation of equilibrium was strongly dependent upon the transverse deflection but only weakly influenced by the in-plane displacement. Conversely, the in-plane equation of equilibrium was strongly dependent upon both the transverse and in-plane deflections. Consequently, the rate of convergence of the transverse nodal equations was much more rapid than the in-plane ones.

In contrast to the treatment of the equations of equilibrium as a typical boundary value problem, the solution for the changes to the moment and force resultants between successive states of quasi-static equilibrium is handled as an initial value problem. As such, a fourth order Runge-Kutta integration routine was employed to integrate the constitutive law at a preselected set of points across the cross section for each axial node used in the finite difference mesh. In this process, it was assumed that the change in actual stress at each of these points could be approximated as a linear function of time over a given, reasonably short, time interval.

Once the "trial stresses" at the end of the time interval had been approximated, a Newton-Cotes quadrature formula was used to numerically approximate the force and moment resultants. These results were then employed to compute the deflections associated with this new state of quasi-static equilibrium. From this deflection solution, a revised actual stress field could be calculated and compared with that which had been employed to integrate the constitutive law. If more than nominal differences existed between the assumed changes in actual stress and those computed, the linear approximating functions were adjusted and the entire process repeated. Otherwise, the results were accepted and the analysis proceeded on to the next time increment.

Generally, it was found that after the first few time steps, this procedure worked very well. Most of the computation effort was expended in the solution of the "boundary value" part of the problem and not in the repetitive iteration of the material behavior. Principally, this was due to the fact that the rate of change in actual stress was reasonably constant and was therefore easy to estimate between successive increments. Where this began to break down, however, was when the behavior of the material began to resemble a classical plastic response. Under these conditions, the rate of change in actual stress would change rapidly even over very short time intervals. Consequently, accurate forecasting its rate of change was more difficult and therefore a greater number of iterations was needed to close the numerical loop.

NUMERICAL RESULTS

The sample problems considered are an eccentrically loaded cantilever beam-column and a simply supported pressure loaded shallow circular arch. In both cases, the behavior of the structural element is examined for constant loading with constant temperatures of 400, 600 and 800 ° C and with sinusoidal temperature variations about the temperatures of 400 and 600 ° C. Simultaneous variations in loading and temperature are not examined. However, the potential influences of time-invariant temperature gradients in the depth direction are examined for both the constant and variable temperature cases.

The beam-column considered is 30.48 cm long having a square cross section of 1.27 cm depth and thickness. The eccentric load is applied 0.3048 cm below the centroidal axis yielding an eccentricity ratio of 0.01. The direction of the load is assumed to remain constant. Twelve axial nodes are used to model the beam-column. Additionally, a five point transverse grid is employed at each axial node to approximate variations in stress and strain across the cross section. One transverse grid point is located at each extreme surface of the cross section and one is positioned on the centroidal axis. The remaining two points are spaced equidistantly between these three points. It should be noted that the results from this "twelve axial node five grid" model compare favorably with results obtained using greater numbers of axial nodes and transverse grid points.

The circular arch examined is a 8.59 deg. segment of a circle. Physically, the arc length of the arch is 22.86 cm with an initial radius of curvature of 152.4 cm. For this relatively shallow arch the rise of the centroidal axis is approximately 0.43 cm. Unlike the beam-column, the arch has a rectangular cross section 0.51 cm in width and 0.38 cm in depth. The arch is divided into fourteen segments for the numerical model. Again, a five point transverse grid is established at the location of each axial node. Similar to the beam-column, the results obtained with this "fourteen-segment five transverse grid model" compare favorably with models employing greater numbers of both. Illustrations of the geometry of the beam-column and arch models are provided in Figs. 3 and 4.

At the outset, it is noted that the particular dimensions selected for these sample problems are not based upon the consideration of "typical" structural elements. Instead, the dimensions are specifically chosen to accelerate the onset of time-dependent behavior. The purpose of this is to minimize the length of the initial "stable" response period thereby reducing the overall magnitude of the computational effort. In general, a "realistically" sized structural element would be appreciably stiffer and thus provide a much longer period of stable response. However, other than this extension of the "stable" useful life, the behavioral characteristics of such "realistic" structural elements would be highly similar to those of the example problems.

Finally, before proceeding with a detailed discussion of the numerical results, some introductory remarks on the principal factors which determine the form of the response merit consideration. Examination of Eqn. (17a), for instance, reveals that the inelastic strain rate is directly determined by the relative magnitudes of the actual stress and the backstress. The inelastic strain rate will change whenever the rate of change in actual stress varies significantly from the rate of change of the backstress. In some situations, the rates of change of actual stress and backstress tend to equilibrate yielding a relatively constant difference between these quantities. With this, the rate of inelastic straining tends to decrease to a nearly constant value leading to a response which may be characterized as initial "primary creep" transitioning to "secondary" or "steady" creep .

However, in other situations, the rate of change in actual stress increases much more rapidly than that of the backstress. Provided the overall magnitude of the difference between them is not excessive, this produces a general response akin to that of accelerating or "terciary" creep. The final possibility occurs when the difference between the actual stress and the backstress is very large. When this happens, the exponential nature of Eqn. (17a) creates a situation where inelastic strain rate tends to follow stress increment directly. Consequently, in the limit, the law exhibits a behavior that may be likened to that of incremental plasticity.

Based on the above, it should be evident that the crucial factors in the analysis are those which determine how rapidly the actual stress and the backstress change with time. The most significant of these factors were found to be a geometrical effect related to the applied bending moment and the growth law for the backstress. Consequently, the overall response of the structural element was found to be determined by the relative interaction between these effects.

The geometric effect occurs in both the beam-column and the arch. However, it is more easily visualized with respect to the beam-column geometry and therefore is described in that context. Essentially, the maximum (in magnitude) stresses in the beam-column are determined by the moment created by the end load. Transverse deflection of the beam-column, increasing the moment arm of the eccentric load, increases the magnitude of these stresses. However, tending to counterbalance this effect is the end rotation. Because the line of action of the load remains constant, end rotation reduces the effective moment arm created by the eccentricity of the load. Thus, this tends to reduce the magnitude of the end moment.

As discussed in a prior study [25], the relative significance of these two opposing influences is related to the amount of eccentricity and the time-dependent characteristics of the material. However, for an eccentricity of the order employed in this study, these two opposing effects can approximately counterbalance one another only when the end deflection is relatively minor. Consequently, beyond this threshold, the transverse deflection effect predominates and the end moment inherently increases. Therefore, the magnitudes of the maximum stresses increase with deflection and thus also with time.

In contrast, for slowly varying temperature changes, allowing the $\dot{\Theta}$ terms of Eqn. (17b) to be neglected, the evolution of the backstress is governed by a relationship of the form

$$\dot{\Omega}_{11} = n_2 \dot{\epsilon}_c - (\Omega_{11} - \Omega^o_{11})\dot{G} \tag{26}$$

With reference to Eqn. (17e), it should evident that $\dot{G}$ must be non-negative. Thus, the magnitude

of the rate of change of the backstress depends upon the signs and magnitudes of the inelastic strain rate and the difference between the current and reference values of backstress. Because the actual stress is only indirectly coupled to the backstress, through the elastic and inelastic deformations and the constitutive growth laws, an increase in actual stress does not necessarily generate an equivalent increase in backstress. Thus, the magnitudes of the quantities appearing in Eqn. (26) need not change in equivalent or proportional amounts. As such, the rate of change of backstress may increase, decrease or remain relatively constant, depending upon the current values of the various parameters. Consequently, this provides a very wide variety of possible results.

The Beam-Column at Constant Temperature

The time-dependent deflection of the beam-column at constant temperature provides the simplest demonstration of these effects. Figures 5, 6 and 7 illustrate the relative time-dependent end deflection of the beam-column under constant load for constant temperatures of 400, 600 and 800 ° C, respectively. The magnitude of the loading is expressed in terms of the ratio of the applied load to the Euler load for the perfect configuration, P_e, where $P_e = \pi^2 EI/4L^2$. Note that the Euler load is a function of temperature due to the temperature dependence of the elastic modulus. Also note that the relative transverse deflection (i.e.: the vertical axis) represents the ratio of the time-dependent transverse deflection to the initial elastic deflection. Consequently, these results indicate the relative increase in deflection produced by inelastic straining.

Except for the lowest load at a temperature of 400 ° C, the 400 and 600 ° C beam-column results exhibit a short initial settling period followed by a virtually linear increase in transverse deflection with respect to time. Generally, this type of behavior is synonomous with a response of primary creep transitioning to secondary creep. Not unexpectedly, the higher loadings produce the greater rates of increase. This infers that under these conditions, the difference between the actual stress and the backstress must remain nearly constant with the greater numerical differences occurring at the highest loadings.

This hypothesis is, of course, confirmed by the results presented in Fig. 8, which illustrates the difference between the maximum (in magnitude) actual stress and the backstress for the 400 ° C case.† Note that, due to the combination of bending and axial compressive loading, the maximum (in magnitude) actual stress occurs in the extreme fibers adjacent to the wall on the same side of the centroidal plane as the applied end load.

Thus since, except for some slight initial variations, the difference between the actual stress and backstress remains virtually constant, the right-hand side of Eqn. (17a) effectively is a constant. This yields a constant, and in this particular case, a relatively low rate of inelastic straining. Consequently, this low rate of inelastic straining does not significantly alter the deflection of the beam-column. As such, significant changes in the actual stresses do not occur. Concurrently, the low rate of inelastic straining

† Results for the difference between the maximum (in magnitude) actual stress and the backstress at a 600 ° C constant temperature are not included because they are virtually identical to those of Fig. 8 and are available elswhere [27]. Again, the difference tends to remain relatively constant following a short initial period; the higher differences occurring for the higher end loads.

yields a low the rate of change in backstress. Thus, the combined impact of these effects is to maintain an approximately constant difference between actual stress and backstress.

In contrast to the 400 and 600 ° C results, virtually all levels of loading at an 800 ° C constant temperature produce an accelerating rate of transverse deflection. Only the lowest level of loading produces a steady creep response; all the other higher loadings result in an accelerating rate of deformation. At the two highest load levels, the beam-column deflects so rapidly that it could be considered to have failed almost instantaneously. Of course, in comparing results between these different temperature cases, the significant differences in the time scales of figures should be kept in mind. At the lower temperatures, elapsed time can be expressed in hours whereas at the highest temperature, elapsed time must be indicated in seconds.

The reason why the 800 ° C results are so different from those at the lower temperatures is directly attributable to the behavior of the difference between the actual stress and the backstress at this temperature, illustrated in Fig. 9. Note that, at the lowest load, the initial relaxation is followed by a period of constant difference between the actual stress and backstress. Thus, for only this load, the increase in actual stress resulting from the increasing transverse deflection effectively is counterbalanced by the concurrent growth in the backstress. Higher levels of loading alter the relative rates of growth of these quantities. At higher loads, the rate of increase in actual stress far exceeds that of the backstress. Consequently, this results in increasing the inelastic strain rate, increasing the rate of deflection and thereby further increasing the rate of change of actual stress. The overall process thus reinforces itself, thereby accelerating the approach to failure.

Before proceeding to a discussion of the arch at constant temperature, a few words concerning the initial relaxation are warranted. The "relaxation" process is actually a combination of effects. First, the inelastic deformation tends to limit the rate of increase in the actual stresses at the extreme fibers. Simultaneously, due to the requirements for equilibrium, this transfers load bearing responsibility toward the centroidal axis. Generally, due to the relatively low initial magnitudes of these stresses, this normally does not produce any significant inelastic staining near the centroidal axis.

The exception to this occurs when the behavior of the beam-column is of the type demonstrated in the 800 ° C case. The rapid inelastic straining at the extreme fibers generates significant increases in the magnitudes of the stresses throughout the central core of the beam-column. Thus, appreciable inelastic straining occurs over the majority of the cross section. Therefore, in addition to the interaction between the maximum (in magnitude) actual stress and the backstress, inelastic straining along the centroidal axis begins to strongly influence the overall response. In fact, the form of "failure" which results might be characterized as a viscoelastic analog to a "plastic hinge."

The Arch at Constant Temperature

The behavior of the pressure loaded shallow arch at constant temperatures of 400, 600 and 800 ° C is generally similar to that of the beam-column. Figures 10 and 11, for example, illustrate the transverse deflection at the center of the arch for pressure loadings at the 600 and 800 ° C temperatures. Employing the solution method described herein, the critical load is estimated to lie between 179 to 186 kPa (26 to 27 psi).

Again, the increase in temperature from 600 to 800 ° C reduces useful life by more than an order

of magnitude. This is, of course, readily apparent from the significant difference in time scale between these two figures. The differences between the actual stress and the backstress for these arch examples are similar to the those provided for the beam-column and thus have not been included.

One common factor to both temperatures is, however, the sensitivity of the results to load magnitude. Note that only a slight increase in pressure can substantially alter the character of the response. The reason for this is that in the arch, unlike the beam-column, the centroidal axis stress is always significant and therefore it always influences behavior. Essentially, due to the curvature, the assumed boundary conditions and the requirements of equilibrium, significant compressive stessing occurs at the centroidal axis. This induces a high rate of compressive inelastic straining along the centroidal axis thereby "reducing" the nominal arc length of the arch. This geometric change tends to accomodate additional transverse deflection through reduction of both the "nominal" curvature and the "unloaded" arc length of the arch. Note also that, unlike the beam-column where such an effect is localized near the wall, this centroidal axis straining occurs over a significant part of the central section of the arch. Thus, the "failure" zone tends to be distributed and not localized. This is why the sudden rapid increase in transverse deflection which occurs with the beam-column is not as pronounced in the arch.

The Influence of Time-Invariant Temperature Gradients

The influence of a time-invariant, linear (in the depth direction) temperature gradient on the constant temperature response is the next factor considered. This type of temperature gradient is typically associated with a steady state constant flow of heat through the depth. For simplicity, the gradient is assumed to remain constant with respect to the length of the element.

For bookkeeping purposes, temperature gradients for which the temperature is greatest at the upper surface and lowest at the bottom surface are considered to be "positive." Conversely, a situation where the greatest temperature is at the bottom surface is denoted as a "negative" gradient. Finally, note that all the gradients were established so that the temperature of the centroidal axis would remain at the nominal case temperature of 400, 600 or 800 $^{\circ}$C. Thus, a +10 $^{\circ}$C gradient for a 400 $^{\circ}$C beam-column implies that the upper, centroidal and lower surface temperatures are 405, 400 and 395 $^{\circ}$C, respectively.

The existence of this type of temperature gradient introduces two effects. First, due to the temperature dependence of the elastic modulus, the first integral of the elastic modulus over a cross section does not vanish. Thus, this introduces a weak level of bending-stretching coupling into the governing equations. The second effect is that such gradients cause thermal bending of the element. Positive gradients cause downward bending thereby augmenting the initial mechanically induced bending. Conversely, a negative gradient reduces the load induced bending of the element.

In general, it was found that neither of these effects exert a major influence on the constant temperature behavior. Figure 12, for example, illustrates the typical relative increase in transverse deflection resulting from a depth direction temperature gradients for the 400 $^{\circ}$C beam-column at a load ratio of 0.50. Note that temperature difference a of +10 or −10 $^{\circ}$C through the 1.27 cm thick beam-column represents a gradient of ± 7.87 $^{\circ}$C/cm. The largest temperature difference considered, namely ± 25 $^{\circ}$C, corresponds to a heat flux through the depth on the order of 400 kW/m^2 $^{\circ}$C.

As mentioned above, Fig. 12 provides the relative increase in deflection. In this particular context,

the relative deflection denotes the ratio of the time-dependent deflection for a given temperature difference to the initial elastic deflection of the uniform temperature beam-column. Thus, this ratio indicates the gross amount of amplification resulting from inelatic and thermo-elastic effects.

In general, temperature differences of 5 ° C and less has little overall impact on the deflection of the constant temperature beam-columns. The +10 ° C and larger temperature differences did, however, have some impact on the transverse deflection. Typically, gradients of these magnitudes generated observable increases in the deflection after several hours of loading. Figure 13 provides a typical example of this employing results obtained for a 600 ° C beam-column with an applied load ratio of 0.50. The solid line represents the initial ratio of end deflection with a thermal gradient to that of the zero gradient case. The dashed lined provides the same ratio after 12.5 hours of loading. Note that, in general, although the deflection of the beam-column is modified due to the presence of the thermal gradient, the magnitude of this change is not sufficient to alter the occurance of the general behaviors illustrated in Figs. 8 through 11. These results are typical of the behavior observed for the other constant temperature beam-column and arch examples which were examined.

As mentioned above, the imposition of such thermal gradients also creates some weak bending-stretching coupling in the governing equations. This also is found to be an insignificant effect. Specifically, a number of temperature gradient test cases where the coupling term, E_1, was artifically set to zero were examined. There was no appreciable difference in the results obtained from these cases compared to results obtained when the coupling term was retained. Consequently, it can be concluded that the potential bending-stretching coupling which might be induced by the temperature dependence of the elastic modulus is negligible.

Arch and Beam-Column Variable Temperature Behavior

The final aspect of behavior examined is the response of the arch and beam-column under sinusoidally varying temperatures. Results are presented for both the arch and beam-column without a time-invariant temperature gradient in the depth direction. The combined influences of sinusoidal temperature variations and a time-invariant depth direction thermal gradient are investigated only for the case of the beam-column.

In the cases examined the temperature is assumed to vary in a sinusoidal manner about an elevated mean temperature of either 400 or 600 ° C. Amplitudes of 50, 100 and 150 ° C are employed in this study. Also, in keeping with the utilization of a quasi-static analysis, 1200 and 1800 sec periods are employed for the sinusoids. Sinusoidal variations about the 800 ° C temperature were not studied due to the extremely short useful life which was exhibited in the constant temperature cases.

Finally, the thermal model includes a slight initial delay between when the load is first applied and when the sinusoidal temperature variations commence. Typically, with some combinations of higher temperatures and higher loads, a step-like initial transient is generated in the constitutive law state variables. Superimposing the start of a sinusoidal temperature at the same time that this step-like increase in the state variables occurs tends to force the Runge-Kutta integration routine to employ exceptionally small time step increments to provide accurate results. However, the need to employ such small time step increments, which substantially increases the overall computational burden, passes almost immediately once the transient change has taken place. Thus, the inclusion of this short delay

allows the integration routine to stabilize before the start of the temperature oscillations. Typically, a delay period on the order of 50 sec is employed. Based on a limited series of test cases, it was found that such a short delay period has no appreciable impact on the overall results.

Figures 14 and 15 illustrate the time dependent deflection of the arch and the beam-column, respectively, for 50 and 100 ^{o}C amplitude temperature oscillations about a 600 ^{o}C temperature. Note that the loading employed in both of these cases would nominally produce a "stable" time-dependent response under constant temperature conditions. Several interesting features can be discerned on these figures. First, the shape of each deflection curve is a distorted sinusoid. The upper peaks tend to be exaggerated whereas the lower peaks are well rounded. Additionally, a distinct underlying increasing trend in time-dependent deflection can be observed in both. Specifically, both the upper peak and lower peak deflections increase between each cycle.

The distortion of the peaks from that of a true sinusoid is a result of the temperature dependence of the inelastic strain. During the higher temperature portion of the cycle, inelastic straining increases due to the temperature sensitivity of the constitutive law parameters. This results in a rapid increase in the deflection. Conversely, at lower temperatures, the inelastic strain rate is reduced. Thus, little inelastic deformation occurs during this part of the cycle. Consequently, the behavior during the lower portion of the temperature cycle closely approximates that of a simple thermo-elastic deformation, where deflection would follow the thermal cycle exactly.

Tables I and II summarize these increasing trends for the arch and beam-column cases, respectively. Note that these tables present results obtained for a variety of temperature differences in the depth direction.

Table I. Rate of Change of Arch Deflection for Sinusoidal Temperature Variations

Pressure (kPa)	Sine Amplitude ^{o}C	Rate of Change (cm/sec) 1^{st} to 2^{nd} Upper Peak	1^{st} to 2^{nd} Lower Peak
165	25	3.18×10^{-7}	2.74×10^{-7}
165	50	3.84×10^{-7}	3.20×10^{-7}
165	100	4.98×10^{-6}	2.87×10^{-6}
152	100	7.87×10^{-7}	6.12×10^{-7}

As Table I illustrates, the magnitude of the increase in deflection between the first and second upper peaks appreciably exceeds that between the first and second lower peaks. Although not indicated in this or the following table, the increase in deflection at the midpoint temperature of the cycle does

fall between the values of the extremes. It should be noted that this unequal expansion of the thermal cycle deflection indicates that a form of creep ratchetting behavior is occurring.

This table also demonstrates the significant nonlinearity involved in this phenomena. Note that the first doubling of the amplitude of the thermal cycle, from 25 to 50 °C, only results in a modest increase in the peak to peak deflections. However, a second doubling, from 50 to 100 °C, increases the peak to peak deflection by slightly more than an order of magnitude. Table II illustrates that a similar effect occurs for the beam-column. Note that except for the 50 °C amplitude without a temperature gradient, increasing the amplitude of the thermal cycle increases the change in peak to peak deflection. Again, the increases occur in a nonlinear manner.

Table II also demonstrates that the increase in deflection between consecutive peaks has an overall decreasing trend. Namely, the absolute increase in deflection decreases as the number of cycles increases. The cause of this decreasing trend is attributed to the growth in backstress. Generally, the maximum actual stresses do not change significantly between consecutive peaks of the thermal cycle. This is because they are principally determined by the thermo-elastic deformation of the element. The accumulated inelastic deformation does not significantly alter this stress distribution. However, the amount of inelastic strain is sufficient to create an increase in the backstress between consecutive peaks, which exceeds that of the actual stress. Consequently, for any particular temperature of the thermal cycle, the difference between the actual stress and the backstress decreases. Thus, the rate of inelastic straining is reduced. Of course, this effect would ultimately cease to be significant once the backstress approaches saturation.

Table II. Rate of Change of Beam-Column Deflection for Sinusoidal Temperature Variations

Sine Ampl.	Temp. Diff.	Rate of Change (cm/sec)			
		Upper Peaks		Lower Peaks	
°C	°C	1^{st} to 2^{nd}	2^{nd} to 3^{rd}	1^{st} to 2^{nd}	2^{nd} to 3^{rd}
50	0	$1.48\text{x}10^{-8}$	$1.27\text{x}10^{-8}$	$1.48\text{x}10^{-8}$	$1.27\text{x}10^{-8}$
50	+10	$8.46\text{x}10^{-8}$	$8.26\text{x}10^{-8}$	$8.05\text{x}10^{-8}$	$7.82\text{x}10^{-8}$
50	+20	$4.29\text{x}10^{-7}$	$4.06\text{x}10^{-7}$	$4.01\text{x}10^{-7}$	$3.84\text{x}10^{-7}$
100	0	$1.07\text{x}10^{-6}$	$1.03\text{x}10^{-6}$	$9.83\text{x}10^{-7}$	$9.45\text{x}10^{-7}$
100	+10	$2.21\text{x}10^{-6}$	$2.06\text{x}10^{-6}$	$2.01\text{x}10^{-6}$	$1.88\text{x}10^{-6}$
100	+20	$4.72\text{x}10^{-6}$	$4.27\text{x}10^{-6}$	$4.24\text{x}10^{-6}$	$3.86\text{x}10^{-6}$
150	0	$1.87\text{x}10^{-5}$	$1.66\text{x}10^{-5}$	$1.61\text{x}10^{-5}$	$1.45\text{x}10^{-5}$
150	+10	$3.22\text{x}10^{-5}$	$2.91\text{x}10^{-5}$	$2.77\text{x}10^{-5}$	$2.52\text{x}10^{-5}$
150	+20	$5.41\text{x}10^{-5}$	$4.93\text{x}10^{-5}$	$4.67\text{x}10^{-5}$	$4.32\text{x}10^{-5}$

The remaining influence illustrated by the data of Table II is the effect that the imposition of a time-invariant depth direction temperature gradient has on the thermal cycle inelastic response. In general, the change in peak to peak deflection is significantly greater in the presence of the time-invariant temperature gradient. Typically, almost an order of magnitude increase in peak to peak change in

deflection occurs for the lowest temperature cycle amplitude. Interestingly, the effect of the depth direction gradient thereafter becomes less significant as the amplitude of the thermal cycle increases.

The ultimate significance of this effect lies in whether or not temperature gradients in the depth direction are truly negligible. The data of this table tend to indicate that the depth direction gradient may not be a negligible factor, when the magnitude of the gradient is of the same relative magnitude as the thermal cycle. In such cases, the thermal gradient does appear to exert an appreciable influence on the overall response. Obviously, this also tends to imply that the impact of the depth direction gradient is potentially very significant in transient cases. In such situations, the magnitude of the temperature difference through the depth can easily approach that of the gross transient change in temperature.

CONCLUSIONS

The elevated temperature behavior of generic types of structural elements fabricated from a typical aerospace alloy have been studied analytically by using a nonlinear kinematic analysis to express the geometry of deformation and by employing a recently developed nonlinear unified hereditary constitutive law to express the time-temperature dependence for the material. The results of this study have demonstrated that, due to the specific format of the constitutive law, the behavioral response of the structural element is determined principally by the difference between the actual stress in the structural element and the backstress state variable of the constitutive law. The first of these, the actual stress in the element, is basically controlled by the geometry of deformation. However, the second factor, the backstress, is governed by the appropriate growth rules of the constitutive law itself.

This implies that accurate results for such an analysis can be obtained only if the form of the backstress growth law and the numerical values employed therein have themselves been established to a reasonably high degree of certainty. Otherwise, the prediction of the conditions under which the response of the structural element may change from that of a "steady stable" form of creep to a rapid approach to failure will not be able to be established with any degree of reliability. For entirely similar reasons, the actual stresses in the structural element also need to be established accurately to ensure that reliable results ensue.

The specific results obtained from the sample problems indicate that a constitutive law of the type proposed by Walker has the capability to model various forms of creep behavior. Under various constant temperature and constant load conditions, it has been shown that the predicted response may vary from that of simple primary creep-secondary creep to that of almost instantaneous occurring terciary creep. Additionally, under varying temperature conditions, the Walker law has demonstrated the capability to predict the development of the type of inelastic strain biasing which can produce creep ratchetting.

Assuming that the Walker law and associated constants provide an accurate representation of the elevated temperature response of a material such as Hastelloy X, the sample problem results also indicate that the existence of a depth-direction temperature gradient in a thin section may not always be negligible. Specifically, under constant temperature conditions, the results indicate that such temperature gradients do not appear to exert any significant influence on behavioral response. However, such gradients do have a significant impact when the overall temperature of the element is not constant. The existence of this type of gradient can appreciably accelerate the overall rate of creep. It is indicated that

this specific effect is most pronounced when the magnitude of the temperature difference through the depth of the element is on the order of the amplitude of the gross variation in temperature of the element. Consequently, in addition to when such conditions may exist in a "quasi-steady state" situation, this implies that such gradients may exert considerable influence in transient thermal problems.

Acknowledgement

The work was performed under NASA Grant NAG 3-534. The financial support provided by NASA is gratefully acknowledged by the authors. The authors also wish to express their appreciation to Dr. C.C. Chamis of the NASA Lewis Research Center for his encouragement and for the numerous technical discussions. Finally, the authors wish to thank Dr. R. Riff of the School of Aerospace Engineering at the Georgia Institute of Technology for his assistance in relaying drafts of this article back and forth between them.

References

1. Hilton, H.H., "Creep Collapse of Viscoelastic Columns With Initial Curvature," Journal of the Aeronautical Sciences, Vol. 19, No. 12, 1952, pp. 844–846.
2. Libove, C.' "Creep Buckling of Columns," Jounal of the Aeronautical Sciences, Vol. 19, No. 7, 1952, pp. 459–467.
3. Odqvist, F.K.G., "Influence of Primary Creep on Column Buckling," Journal of Applied Mechanics, Vol. 21, No. 3, 1954, pp 295.
4. Hoff, N.J., "Creep Buckling," The Aeronautical Quarterly, Vol. 7, No. 1, 1956, pp. 1–20.
5. Miller, D.R., "Thermal Stress Ratchet Mechanism in Pressure Vessels," ASME Journal of Basic Engineering, Vol. 81, 1959, pp. 190–196.
6. Edmunds, H.G. and Beer, F.J., "Notes on Incremental Collapse in Pressure Vessels," Journal of Mechanics and Engineering Science, Vol. 5, 1961, pp. 187–199.
7. Bree, J. "Elastic Plastic Behavior of Thin Tubes Subjected to Internal Pressure and Intermittent High Heat Fluxes," Journal of-Strain Analysis, Vol. 2, 1967, pp. 226–238.
8. Bree, J., "Incremental Growth Due to Creep and Plastic Yielding of Thin Tubes Subjected to Internal Pressure and Cyclic Thermal Stresses," Journal of Strain Analysis, Vol. 3, 1968, pp. 122-127.
9. Conway, J.B., Berling, J.T., Stentz, R.H., Pugh, C.E. and Anderson, W.F., "Thermal Ratchetting Studies of Type 304 Stainless Steel - An Evaluation of a New Test Procedure," Symposium on Structural Materials for Service at Elevated Temperatures in Nuclear Power Generation, ASME 1975 Winter Annual Meeting, Houston, Texas, pp. 247–281.
10. Corum, J.M., Young, H.C. and Grindell, A.G., "Thermal Ratchetting in Pipes Subjected to Intermittent Thermal Downshocks at Elevated Temperature," Oak Ridge National Laboratory, Tennessee, 1974.
11. Corum J.M., Richardson, M. and Clinard, J.A., "Elevated-Temperature Benchmark Tests of Simply Supported Circular Plates Subjected to Time-Varying Loadings," Oak Ridge National Laboratory, Tennessee, 1977

12. Mukherjee, S., Kumar, V., and Chang, K.J., "Elevated Temperature Inelastic Analysis of Metallic Media Under Time Varying Loads Using State Variable Theories," International Journal of Solids and Structures, Vol. 14, 1978, pp. 663–679.

13. Hart, E.W., "Constitutive Relations for the Npnelastic Deformation of Metals," Journal of Engineering Materials and Technology, Vol. 98, 1976, pp. 193–202.

14. Hart, E.W., "A Micromechanical Basis for Constitutive Equations with Internal Variables," Journal of Engineering Materials and Technology, Vol. 106, 1984, pp. 322–325.

15. Pointer, A.R.S. and Leckie, F.A., "Constitutive Relationships for the Time Dependent Deformation of Metals," Journal of Engineering Materials and Technology, Vol. 98, 1976, pp. 47–51.

16. Pugh, C.E. and Robinson, D.N., "Some Trends in Constitutive Equation Model Development for High-Temperature Behavior of Fast-Reactor Structural Alloys," Nuclear Engineering Design, 1978, pp. 269–276.

17. Pugh, C.E. and Robinson, D.N., "Constitutive Equations for Meeting Elevated-Temperature-Design Needs," ASME Pressure Vessel and Piping Conference, Denver, Colorado, 1981.

18. Pugh, C.E., "Progress in Developing Constitutive Equations for Inelastic Design Analysis," Journal of Pressure Vessel Technology, Vol. 105, 1983, pp. 273–276.

19. Krempl, E., "On the Interaction of Rate and History Dependence in Structural Metals," Acta Mechanica, Vol. 22, 1975, pp. 53–90.

20. Walker, K.P. and Krempl. E., "An Implicit Functional Theory of Viscoplasticity," Mechanics Research Communications, Vol. 5, No. 4, 1978, pp. 179–184.

21. Corum, J.M. and Sartory, W.K., "Assessment of Current High-Temperature Design Methodology Based on Structural Failure Tests," Journal of Pressure Vessel Technology, Vol. 109, 1987, pp. 160–168.

22. Walker, K.P., "Research and Development Program for Nonlinear Structural Modeling with Advanced Time-Temperature Dependent Constitutive Relationships," United Technologies Research Center, NASA Contract Report NASA-CR-165533, 1981.

23. Moreno, V., "Development of a Simplified Analytic Method for Representing Material Cyclic Response," United Technologies Research Center, NASA Contract Report NASA-CR-168100, 1983.

24. Moreno, V., "Combustor Durability Analysis," United Technologies Research Center, NASA Contract Report NASA-CR-165250, 1981.

25. Stubstad, J.M. and Simitses, G.J., "Bounding Solutions for Geomertically Nonlinear Viscoelastic Problems," AIAA Journal, Vol. 24, No. 11, 1986, pp. 1843–1850.

26. Thurston, G., "Newton's Method Applied to Problems in Nonlinear Mechanics," Journal of Applied Mechanics, Vol. 32, 1965, pp. 383-388.

27. Stubstad, J.M., "Nonlinear Thermoviscoelastic Analysis of Metallic Plane Curved Beams," PhD Dissertation submitted in partial fulfillment of the requirements for the degree of Doctor of Philosophy, Georgia Institute of Technology, 1986.

Appendix A Constitutive Law

In its most general integral form, Walker's functional theory has the format:

$$\sigma_{ij}(t) = \frac{2}{3}\Omega_{ij}(t) + \delta_{ij}\int_o^t \left(\lambda[\Theta(\xi)] + \frac{2}{3}\mu[\Theta(\xi)]\right)\left(\frac{\partial \epsilon_{kk}}{\partial \xi} - 3\alpha[\Theta(\xi)]\frac{\partial \Theta}{\partial \xi}\right) d\xi$$
$$+ \int_o^t e^{-\{Q(t)-Q(\xi)\}}\left(2\mu[\Theta(\xi)]\frac{\partial \epsilon_{ij}}{\partial \xi} - \frac{2}{3}\delta_{ij}\mu[\Theta(\xi)]\frac{\partial \epsilon_{kk}}{\partial \xi} - \frac{2}{3}\frac{\partial \Omega_{ij}}{\partial \xi}\right) d\xi, \qquad (A-1a)$$

$$\Omega_{ij}(t) = \Omega^o_{ij}(t) + n_1[\Theta(t)]c_{ij}(t) + n_2[\Theta(t)]\int_o^t e^{-\{G(t)-G(\xi)\}}\frac{\partial c_{ij}}{\partial \xi} d\xi, \qquad (A-1b)$$

$$K(t) = K_1[\Theta(t)] - K_2[\Theta(t)]e^{-n_7[\Theta(t)]W(t)}, \qquad (A-1c)$$

$$c_{ij} = \int_o^t \frac{1}{2\mu}\left(\delta_{ij}\lambda[\Theta(\xi)]\frac{\partial \epsilon_{kk}}{\partial \xi} + 2\mu[\Theta(\xi)]\frac{\partial \epsilon_{ij}}{\partial \xi} - \frac{\partial \sigma_{ij}}{\partial \xi}\right.$$
$$\left. - \delta_{ij}\alpha[\Theta(\xi)]\left(3\lambda[\Theta(\xi)] + 2\mu[\Theta(\xi)]\right)\frac{\partial \Theta}{\partial \xi}\right) d\xi, \qquad (A-1d)$$

$$\Omega^o_{ij} = -\Omega^o[\Theta(t)]\left(\delta_{ij} - 3\frac{c_{ik}(t)c_{kj}(t)}{c_{pq}(t)c_{pq}(t)}\right), \qquad (A-1e)$$

$$Q(t) = \int_o^t \frac{3\mu[\Theta(\xi)]}{K(\xi)}\left(\frac{\partial W}{\partial \xi}\right)^{1-1/n[\Theta(\xi)]} d\xi, \qquad (A-1f)$$

$$G(t) = \int_o^t \left\{ \left(n_3[\Theta(\xi)] + n_4[\Theta(\xi)]e^{-n_5[\Theta(\xi)]W(\xi)}\right)\frac{\partial W}{\partial \xi}\right.$$
$$\left. + n_6[\Theta(\xi)]\left(\frac{2}{3}\Omega_{ij}(\xi)\Omega_{ij}(\xi)\right)^{(m[\Theta(\xi)]-1)/2}\right\} d\xi, \qquad (A-1g)$$

and

$$W(t) = \int_o^t \sqrt{\frac{2}{3}\frac{\partial c_{ij}}{\partial \xi}\frac{\partial c_{ij}}{\partial \xi}}\, d\xi. \qquad (A-1h)$$

Square bracket terms, of the form $\mu[\Theta(t)]$, are used to denote the dependence of the material constants λ, μ, Ω^o, n, m, n_1, n_2, n_3, n_4, n_5, n_6, n_7, K_1, and K_2 on the temperature, Θ. However, for clarity, the indication of the explicit dependence on temperature will be suppressed in the following development.

The differential format for Walker's functional theory is obtained through differentiating the above relations with respect to time. Employing Leibniz's rule, differential formats for Eqns. (A-1d), (A-1f), (A-1g) and (A-1h) are readily obtained. A somewhat simplified differential format for Eqn. (A-1b) may be obtained in the following manner. Differentiating Eqn. (A-1b) with respect to time and using Leibniz's rule, after rearranging, yields

$$\dot{\Omega}_{ij} = \dot{\Omega}^o_{ij} + (n_1 + n_2)\dot{c}_{ij} + c_{ij}\frac{\partial n_1}{\partial \Theta}\dot{\Theta} + \left[\frac{\partial n_2}{\partial \Theta}\dot{\Theta} - n_2\dot{G}\right]\int_o^t e^{-\{G(t)-G(\xi)\}}\frac{\partial c_{ij}}{\partial \xi}. \qquad (A-2)$$

The integral which appears in the above is identical to the integral of Eqn. (A-1b). Consequently, solving Eqn. (A-1b) for the integral and substituting into Eqn. (A-2) yields the differential format given by Eqn. (A-6b).

With some manipulation, the differential form of Eqn. (A-1a) may be stated in a "power law" type format. First, Eqn. (A-1a) is differentiated with respect to time and then simplified using the deviatoric stress tensor to yield

$$\frac{2}{3}\left(\frac{3}{2}s_{ij}-\Omega_{ij}\right)=\int_o^t e^{-\{Q(t)-Q(\xi)\}}\left[2\mu\frac{\partial\epsilon_{ij}}{\partial\xi}-\frac{2}{3}\mu\delta_{ij}\frac{\partial\epsilon_{kk}}{\partial\xi}-\frac{2}{3}\frac{\partial\Omega_{ij}}{\partial\xi}\right]d\xi. \qquad (A-3)$$

Note that to establish the above it is necessary to show that $\Omega_{kk}=\Omega^o_{kk}=0$. These, however, follow directly from Eqns. (A-1b) and (A-1e) provided the inelastic portion of the deformation may be treated as, at least, approximately incompressible (i.e., $c_{kk}\approx 0$).

Therefore, substituting Eqn. (A-3) into Eqn. (A-2) and using the differential form of Eqn. (A-1d) yields:

$$2\mu\dot{c}_{ij}=\frac{2}{3}\dot{Q}\left(\frac{3}{2}s_{ij}-\Omega_{ij}\right). \qquad (A-4)$$

The $\dot{Q}$ term can be replaced with the aid of the differential forms of Eqns. (A-1f) and (A-1h). After some algebraic manipulation and minor rearranging this yields:

$$\dot{W}=\left(\frac{\sqrt{\frac{2}{3}\left(\frac{3}{2}s_{ij}-\Omega_{ij}\right)\left(\frac{3}{2}s_{ij}-\Omega_{ij}\right)}}{K}\right)^n. \qquad (A-5)$$

Consequently, substituting Eqn. (A-5) back into the differential form of Eqn. (A-1f) and using Eqn. (A-4) yields, after some algebra, the differential power law of Eqn. (A-1a). Thus, the complete set of differential relations for Walker's functional theory are:

$$\dot{c}_{ij}=\left(\frac{\sqrt{\frac{2}{3}\left(\frac{3}{2}s_{kl}-\Omega_{kl}\right)\left(\frac{3}{2}s_{kl}-\Omega_{kl}\right)}}{K}\right)^n\frac{\left(\frac{3}{2}s_{ij}-\Omega_{ij}\right)}{\sqrt{\frac{2}{3}\left(\frac{3}{2}s_{mn}-\Omega_{mn}\right)\left(\frac{3}{2}s_{mn}-\Omega_{mn}\right)}}, \qquad (A-6a)$$

$$\dot{\Omega}_{ij}=\dot{\Omega}^o_{ij}+(n_1+n_2)\dot{c}_{ij}+\dot{c}_{ij}\frac{\partial n_1}{\partial\Theta}\dot{\Theta}-(\Omega_{ij}-\Omega^o_{ij}-n_1c_{ij})\left(\dot{G}-\frac{1}{n_2}\frac{\partial n_2}{\partial\Theta}\dot{\Theta}\right), \qquad (A-6b)$$

$$K=K_1-K_2e^{-n_7W}, \qquad (A-6c)$$

$$2\mu\dot{c}_{ij}=\delta_{ij}\lambda\dot{\epsilon}_{kk}+2\mu\dot{c}_{ij}-\dot{\sigma}_{ij}-\delta_{ij}(3\lambda+2\mu)\alpha\dot{\Theta}, \qquad (A-6d)$$

$$\dot{\Omega}^o_{ij}=\frac{\Omega^o_{ij}}{\Omega^o}\frac{\partial\Omega^o}{\partial\Theta}\dot{\Theta}+\frac{3\Omega^o}{(c_{pq}c_{pq})^2}\left[\dot{c}_{ik}c_{kj}c_{pq}c_{pq}+c_{ik}\dot{c}_{kj}c_{pq}c_{pq}-2c_{ik}c_{kj}c_{pq}\dot{c}_{pq}\right], \qquad (A-6e)$$

$$\dot{G} = (n_3 + n_4 e^{-n_5 W})\dot{W} + n_6 \left(\frac{2}{3}\Omega_{ij}\Omega_{ij}\right)^{(m-1)/2}, \qquad (A-6f)$$

and

$$\dot{W} = \sqrt{\frac{2}{3}\dot{c}_{ij}\dot{c}_{ij}}. \qquad (A-6g)$$

Note that a differential form for the function Q is not required since it does not appear in any of the other expressions.

Numerical constants for the law were established [22–24] from uniaxial bar specimens tested under fully reversed, strain-rate controlled cyclic stress-strain tests. These tests were conducted for a variety of temperatures and strain rates. The testing conditions were sufficiently rigorous to cause plastic deformation during the loading cycle. The creep and relaxation properties were deduced from observation of the behavior of the samples when the cyclic loading was "held" at various points on the "steady-state" hysteresis loop. Appendix Figs. A-1 through A-8 illustrate the temperature dependent parametric values established under that work. Note that the material constants K_2, n_1, n_4, n_5, and n are zero over the enitre temperature range considered. This results in additional simplifications to the constitutive law.

Appendix B Finite Difference Equations

Solutions for the governing nonlinear differential equations are obtained using a Newton type method for nonlinear differential equations. It is assumed that trial solutions for the transverse and axial deflection functions, denoted as $\tilde{w}$ and $\tilde{u}$, respectively, exist. From these, trial values for centroidal axis strain and cross section rotation, $\tilde{\epsilon}_o$ and $\tilde{\phi}$, respectively, are determined. Then, using the approximations $\epsilon_o = \tilde{\epsilon}_o + \Delta\epsilon_o$ and $\phi = \tilde{\phi} + \Delta\phi$ to substitute into Eqns. (16) yields

$$\tilde{k}(E_0\Delta\epsilon_o + E_1\frac{\partial\Delta\phi}{\partial s}) - \frac{\partial^2\Delta M}{\partial s^2} = p^* - \tilde{k}\tilde{N} + \frac{\partial^2\tilde{M}}{\partial s^2}, \qquad (B-1a)$$

$$(E_0 + \tilde{k}E_1)\frac{\partial\Delta\epsilon_o}{\partial s} + (E_1 + \tilde{k}E_2)\frac{\partial^2\Delta\phi}{\partial s^2} = -\frac{\partial\tilde{N}}{\partial s} - \tilde{k}\frac{\partial\tilde{M}}{\partial s}. \qquad (B-1b)$$

The terms $\tilde{N}$ and $\tilde{M}$ are evaluated by substituting $\tilde{\epsilon}_o$ and $\tilde{\phi}$ into Eqns. (11). Numerical methods are used to approximate the derivative terms on the right-hand side of Eqns (B-1). The second derivative of the moment correction, which appears on the left-hand side of Eqn. (B-1a), also is evaluated numerically. This avoids the numerical problems which can result in approximating fourth derivatives directly.

Assuming $w = \tilde{w} + \Delta w$ and a similar expansion for u, upon substitution into Eqn. (7) and neglecting terms of order $(\Delta w)^2$ and higher, yields

$$\Delta\epsilon_o = A(\frac{\partial\Delta u}{\partial s} + \kappa\Delta w) + B(\frac{\partial\Delta w}{\partial s} - \kappa\Delta u) \qquad (B-2)$$

where the factors A and B are defined as:

$$A = 1 + \frac{\partial\tilde{u}}{\partial s} + \kappa\tilde{w} \qquad \text{and} \qquad B = \frac{\partial\tilde{w}}{\partial s} - \kappa\tilde{u}. \qquad (B-3a,b)$$

Differentiating Eqn. (B-2) with respect to s yields, after rearranging,

$$\begin{aligned}\frac{\partial \Delta\epsilon_o}{\partial s} =& \mathrm{A}\frac{\partial^2 \Delta \mathrm{u}}{\partial s^2} + (\mathrm{C} - \kappa \mathrm{B})\frac{\partial \Delta \mathrm{u}}{\partial s} - \kappa \mathrm{D}\Delta \mathrm{u}, \\ &+ \mathrm{B}\frac{\partial^2 \Delta \mathrm{w}}{\partial s^2} + (\mathrm{D} + \kappa \mathrm{A})\frac{\partial \Delta \mathrm{w}}{\partial s} + \kappa \mathrm{C}\Delta \mathrm{w}\end{aligned} \qquad (B-4)$$

where C and D are given by

$$\mathrm{C} = \frac{\partial^2 \tilde{\mathrm{u}}}{\partial s^2} + \kappa \frac{\partial \tilde{\mathrm{w}}}{\partial s} \qquad \text{and} \qquad \mathrm{D} = \frac{\partial^2 \tilde{\mathrm{w}}}{\partial s^2} - \kappa \frac{\partial \tilde{\mathrm{u}}}{\partial s}. \qquad (B-5a,b)$$

Developing an expression for $\Delta\phi$ is accomplished by using Eqn. (8). Since it is assumed that $\phi = \tilde{\phi} + \Delta\phi$, substitution into Eqn. (8) yields

$$\sin(\tilde{\phi} + \Delta\phi) \approx \sin\tilde{\phi} + \Delta\phi\cos\phi \approx \frac{\frac{-\partial \tilde{\mathrm{w}}}{\partial s} + \kappa\tilde{\mathrm{u}}}{\sqrt{1 + 2\tilde{\epsilon}_o + 2\Delta\epsilon_o}} + \frac{\frac{-\partial \Delta \mathrm{w}}{\partial s} + \kappa\Delta \mathrm{u}}{\sqrt{1 + 2\tilde{\epsilon}_o + 2\Delta\epsilon_o}} \qquad (B-6)$$

where the approximations $\sin\Delta\phi \approx \Delta\phi$ and $\cos\Delta\phi \approx 1$ have been used. For small $\tilde{\epsilon}_o$ it is reasonable to assume that $\Delta\epsilon_o < \tilde{\epsilon}_o$, thus allowing the $\Delta\epsilon_o$ term to be neglected. Thus, since the first term on the left-hand side, according to Eqn. (8), is equal to the first term of the right-hand side, this implies that

$$\Delta\phi\cos\phi \approx \frac{\frac{-\partial \Delta \mathrm{w}}{\partial s} + \kappa\Delta \mathrm{u}}{\sqrt{1 + 2\tilde{\epsilon}_o}}. \qquad (B-7)$$

Therefore, combining Eqns. (8) and (B-7) yields

$$\Delta\phi \approx \frac{1}{\mathrm{A}}\left(-\frac{\partial \Delta \mathrm{w}}{\partial s} + \kappa\Delta \mathrm{u}\right). \qquad (B-8)$$

Derivatives of $\Delta\phi$ are obtained from Eqn. (B-8). In this, it is assumed that the term 1/A may be treated as an approximate constant and thus need not be differentiated. This provides significant simplifications without engendering any substantial inaccuracies since the correction terms become negligible as the exact solution is approached. Consequently, differentiating Eqn. (B-8) with respect to s yields:

$$\frac{\partial \Delta\phi}{\partial s} \approx \frac{1}{\mathrm{A}}\left(-\frac{\partial^2 \Delta \mathrm{w}}{\partial s^2} + \kappa\frac{\partial \Delta \mathrm{u}}{\partial s}\right), \qquad (B-9a)$$

and

$$\frac{\partial^2 \Delta\phi}{\partial s^2} \approx \frac{1}{\mathrm{A}}\left(-\frac{\partial^3 \Delta \mathrm{w}}{\partial s^3} + \kappa\frac{\partial^2 \Delta \mathrm{u}}{\partial s^2}\right). \qquad (B-9b)$$

Central difference formulae are used to approximate the derivative terms. However, prior to substituting into Eqns. (B-1) it is useful to establish the following definitions:

$$a_i = \tilde{k}_i \mathrm{E}_0 + \frac{2\mathrm{E}_1}{\Delta s^2}, \qquad b_i = \tilde{k}_i \mathrm{E}_1 + \tilde{\mathrm{N}}_i + \frac{2\mathrm{E}_2}{\Delta s^2}, \qquad (B-10a,b)$$

$$c_i = \mathrm{E}_0 + \tilde{k}_i \mathrm{E}_1 \qquad \text{and} \qquad d_i = \mathrm{E}_1 + \tilde{k}_i \mathrm{E}_2. \qquad (B-10c,d)$$

Thus, substituting the various expressions given above into Eqns. (B-1) yields, after rearranging, the general finite difference nodal equations

$$
\begin{aligned}
&\Big(\frac{E_1 A_{i-1}}{2\Delta s^3}+\frac{\kappa E_2}{2A_{i-1}\Delta s^3}\Big)\Delta u_{i-2}+\Big(\frac{\kappa E_1 B_{i-1}}{\Delta s^2}-\frac{a_i A_i}{2\Delta s}-\frac{\kappa b_i}{2A_i\Delta s}\Big)\Delta u_{i-1}\\
&+\Big(-\frac{E_1}{2\Delta s^3}(A_{i-1}-A_{i+1})-\kappa a_i B_i-\frac{\kappa E_2}{2\Delta s^3}\Big(\frac{1}{A_{i-1}}-\frac{1}{A_{i+1}}\Big)\Big)\Delta u_i\\
&+\Big(\frac{a_i A_i}{2\Delta s}+\frac{\kappa E_1 B_{i+1}}{\Delta s^2}+\frac{\kappa b_i}{2\Delta s A_i}\Big)\Delta u_{i+1}-\Big(\frac{E_1 A_{i+1}}{2\Delta^3}+\frac{\kappa E_2}{2A_{i+1}\Delta s^3}\Big)\Delta u_{i+2}\\
&+\Big(\frac{E_1 B_{i-1}}{2\Delta s^3}+\frac{E_2}{A_{i-1}\Delta s^4}\Big)\Delta w_{i-2}\\
&-\Big(\frac{\kappa E_1 A_{i-1}}{\Delta s^2}+\frac{a_i B_i}{2\Delta s}+\frac{2E_2}{A_{i-1}\Delta s^4}+\frac{b_i}{A_i\Delta s^2}\Big)\Delta w_{i-1}\\
&-\Big(\frac{E_1}{2\Delta s^3}(B_{i-1}-B_{i+1})-\kappa a_i A_i-\frac{E_2}{\Delta s^4}\Big(\frac{1}{A_{i-1}}+\frac{1}{A_{i+1}}\Big)-\frac{2b_i}{A_i\Delta s^2}\Big)\Delta w_i\\
&+\Big(\frac{a_i B_i}{2\Delta s}-\frac{\kappa E_1 A_{i+1}}{\Delta s^2}-\frac{b_i}{A_i\Delta s^2}-\frac{2E_2}{A_{i+1}\Delta s^4}\Big)\Delta w_{i+1}\\
&-\Big(\frac{E_1 B_{i+1}}{2\Delta s^3}-\frac{E_2}{A_{i+1}\Delta s^4}\Big)\Delta w_{i+2}=p^*+\frac{\partial^2\tilde{M}_i}{\partial s^2}-\tilde{k}_i-\tilde{N}_i
\end{aligned}
\qquad (B-11)
$$

and

$$
\begin{aligned}
&\Big(\frac{c_i A_i}{\Delta s^2}+\frac{c_i(C_i-\kappa B_i)}{2\Delta s}+\frac{\kappa d_i}{A_i\Delta s^2}\Big)\Delta u_{i+1}-\Big(\frac{2c_i A_i}{\Delta s^2}+\kappa c_i D_i+\frac{2\kappa d_i}{A_i\Delta s^2}\Big)\Delta u_i\\
&+\Big(\frac{c_i A_i}{\Delta s^2}-\frac{c_i(C_i-\kappa B_i)}{2\Delta s}+\frac{\kappa d_i}{A_i\Delta s^2}\Big)\Delta u_{i-1}+\Big(\frac{d_i}{2A_i\Delta s^3}\Big)\Delta w_{i+2}\\
&+\Big(\frac{c_i B_i}{\Delta s^2}+\frac{c_i(D_i+\kappa A_i)}{2\Delta s}-\frac{d_i}{A_i\Delta s^3}\Big)\Delta w_{i+1}+\Big(-\frac{2c_i B_i}{\Delta s^2}+\kappa c_i C_i\Big)\Delta w_i\\
&+\Big(\frac{c_i B_i}{\Delta s^2}-\frac{c_i(D_i+\kappa A_i)}{2\Delta s}+\frac{d_i}{A_i\Delta s^3}\Big)\Delta w_{i-1}-\Big(\frac{d_i}{2A_i\Delta s^3}\Big)\Delta w_{i-2}\\
&=-\frac{\partial\tilde{N}_i}{\partial s}-\tilde{k}_i\frac{\partial\tilde{M}_i}{\partial s}.
\end{aligned}
\qquad (B-12)
$$

These two equations provide the finite-difference approximation for the deflection of the internal nodes of the beam, that is for the subscript i over the range $3 \le i \le n-1$, (see Fig. 4). Therefore, for an arch of $n+1$ total nodes, they provide a system of $2n-6$ equations in $2n+2$ unknowns. Thus, eight additional equations are required to provide a unique solution for the problem. Six of these equations are obtained by using the boundary condition. These provide two sets of three equations, one set applicable to node 1 and the other set for node $n+1$.

As evidenced above, the boundary conditions do not provide a sufficient number of relations to enable unique solution. This, in part, results from the inherent coupling generated by the assumption of Euler-Bernoulli bending when both axial and transverse deflections are possible. Note that the deflection

functions are not only related to one another, but they also appear in the same functional format in both expressions. The derivative of one is added to (subtracted from) the other multiplied by the curvature. This, in turn, indicates that a form of implicit coupling exists between the two generalized displacements, centroidal axis strain and rotation. Ideally, the generalized displacements should be completely independent.

A number of approaches can be employed to generate the two additional equations needed for unique solution. The one used in this study is to require the "centroidal axis" strain in the wall to vanish. Mathematically, this is equivalent to appending, to the existing system of equations, the two additional equations:

$$\Delta\epsilon_{ol} = -\tilde{\epsilon}_{ol} \qquad \text{and} \qquad \Delta\epsilon_{or} = -\tilde{\epsilon}_{or}, \qquad (B-14a,b)$$

where ϵ_{ol} and ϵ_{or} represent the strain in the left and right extensions, respectively. No condition is established for the "rotations" which might occur in the wall sections. This is not felt to be significant since the nodal mesh, at least for the equilibrium problem, is a centroidal mesh.

Using the boundary conditions and the two "wall strain" relations it is possible to eliminate the transverse and axial displacement components for nodes 1, 2, n, and n + 1 from the general finite-difference equations. This leaves a system of exactly 2n − 6 equations in the same number of unknowns. If the coefficients of these equations are arranged in matrix form, the result is a banded matrix with a bandwidth of six.

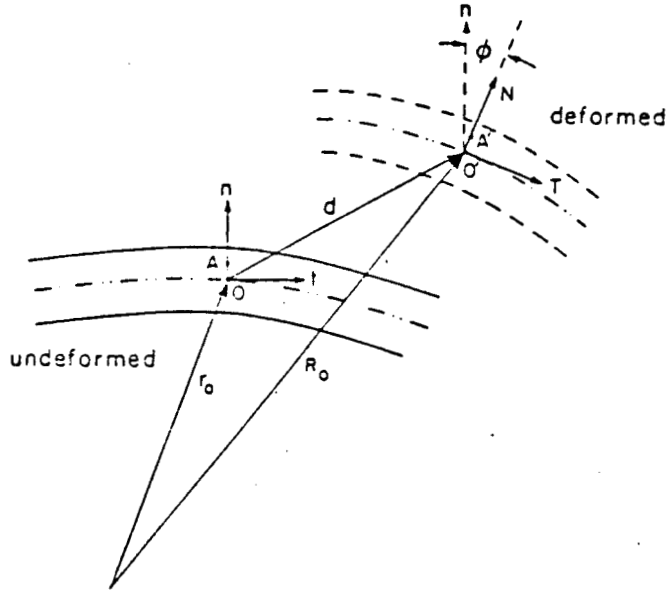

Figure 1. Geometry of Deformation.

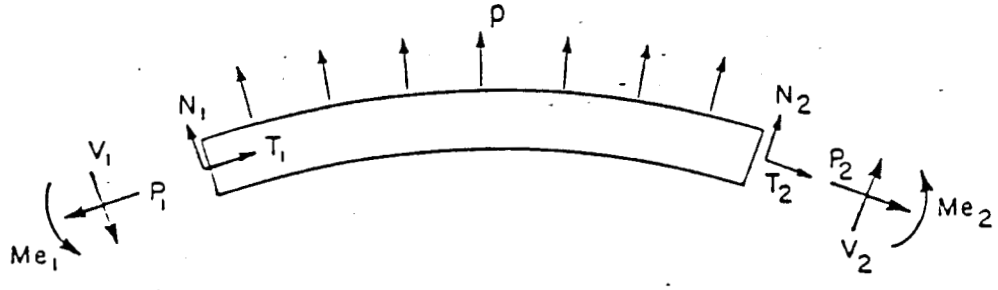

Figure 2 External Forces and Moments Acting on the Arch.

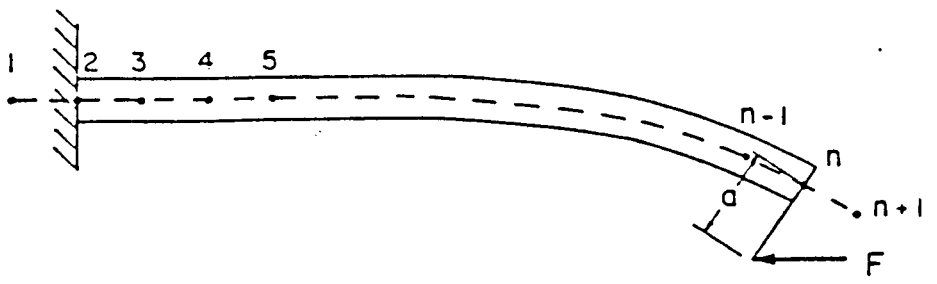

Figure 3 Eccentrically Loaded Cantilever Beam-Column.

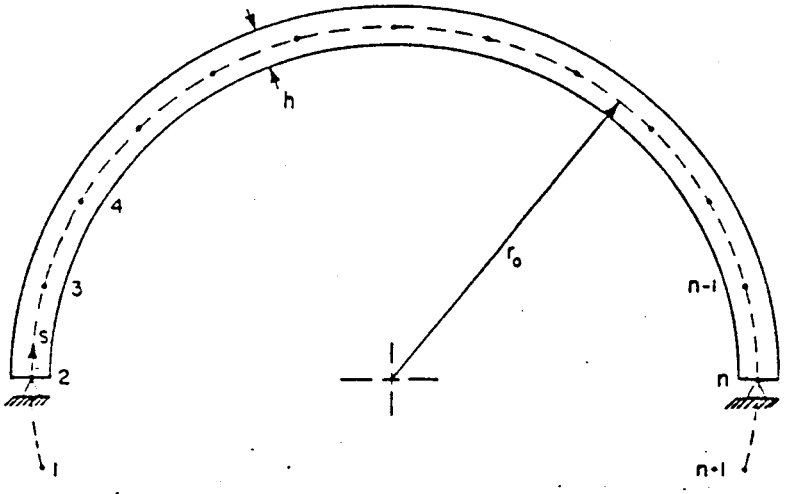

Figure 4 Axial Finite Difference Mesh for the Arch

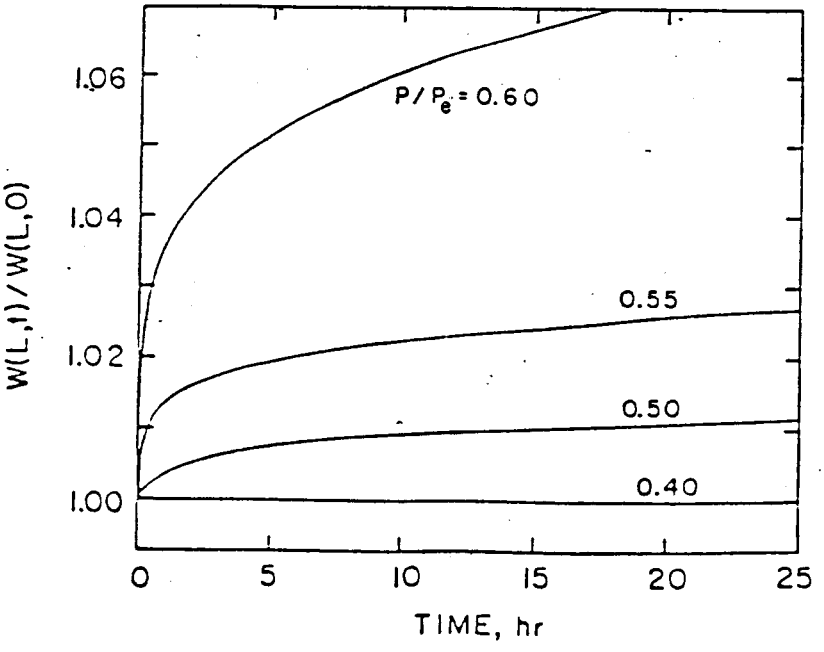

Figure 5 Beam-Column Deflection at 400 °C.

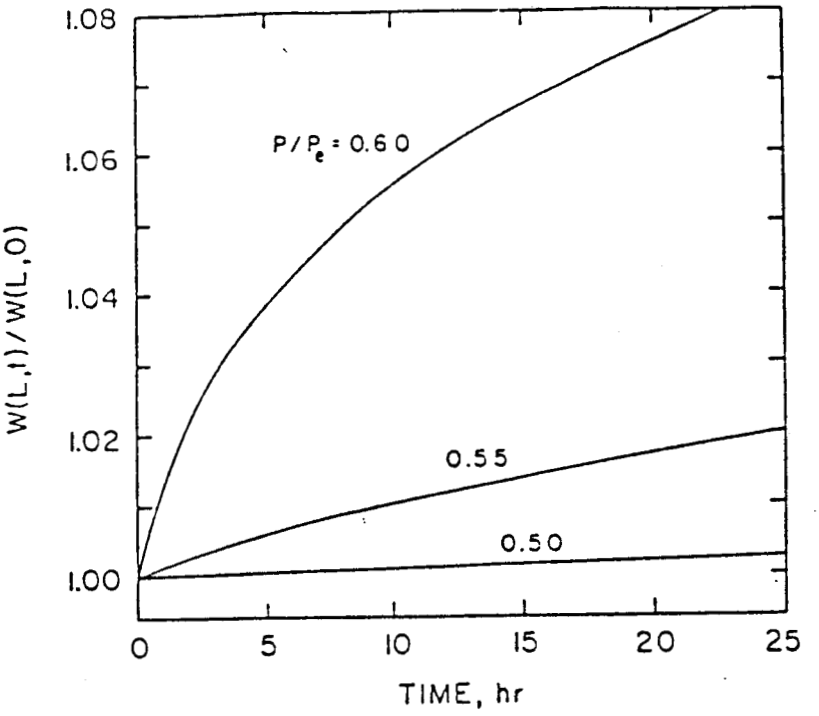

Figure 6 Beam-Column Deflection at 600 °C.

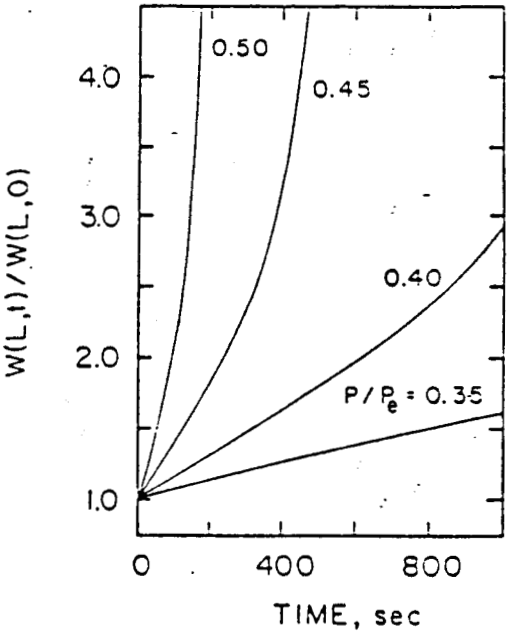

Figure 7 Beam-Column Deflection at 800 °C.

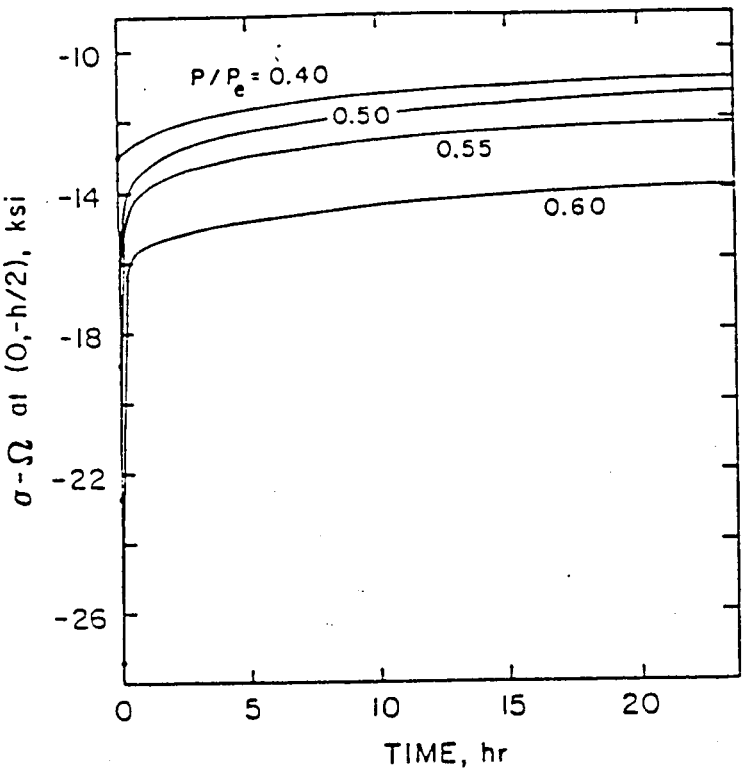

Figure 8 Difference Between Actual Stress and Backstress at 400 °C.

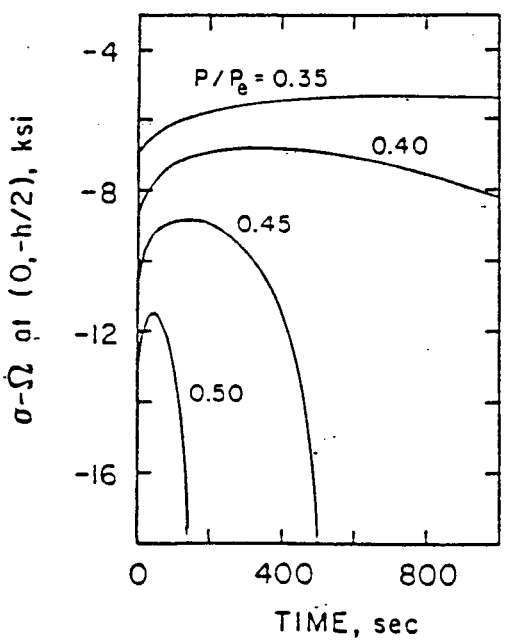

Figure 9 Difference Between Actual Stress and Backstress at 8(

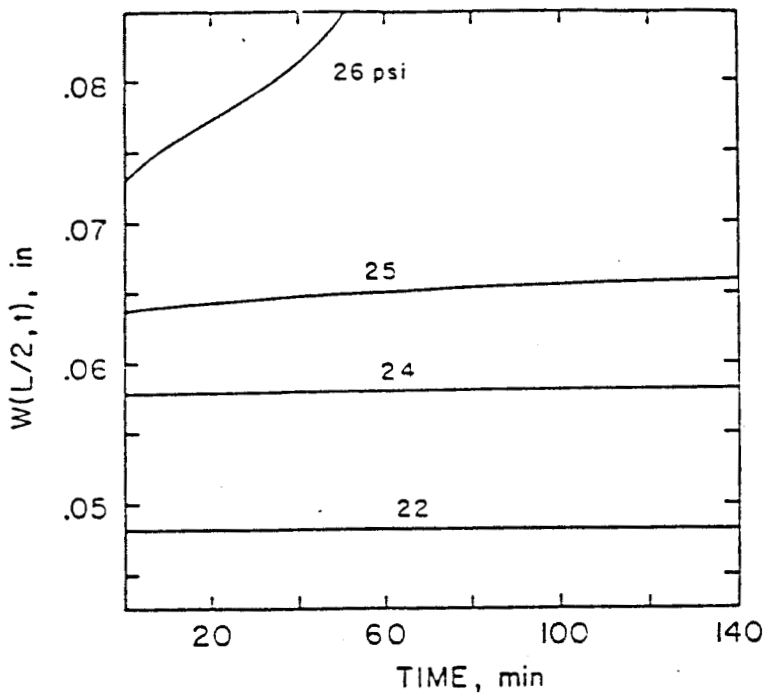

Figure 10 Center Deflection Versus Time for the 600 °C Low Arch.

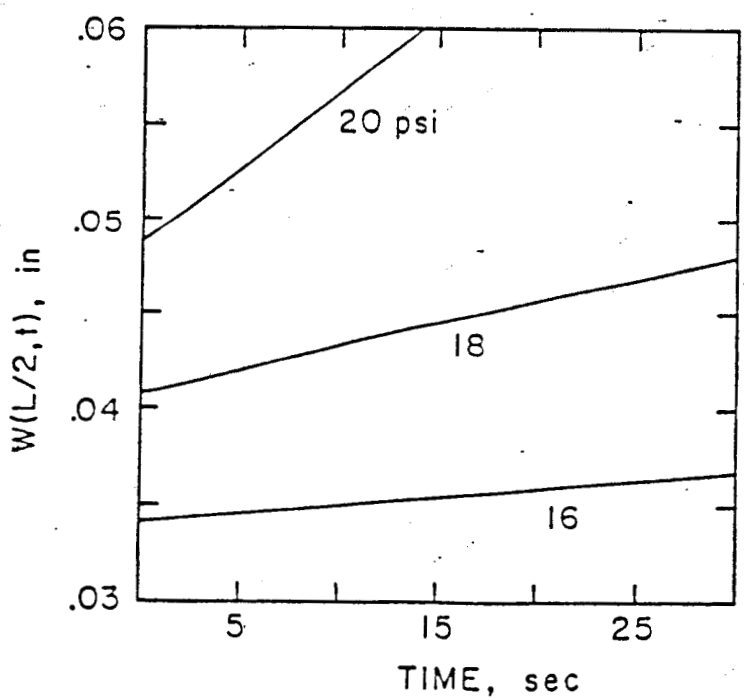

Figure 11 Center Deflection Versus Time for the 800 °C Low Arch.

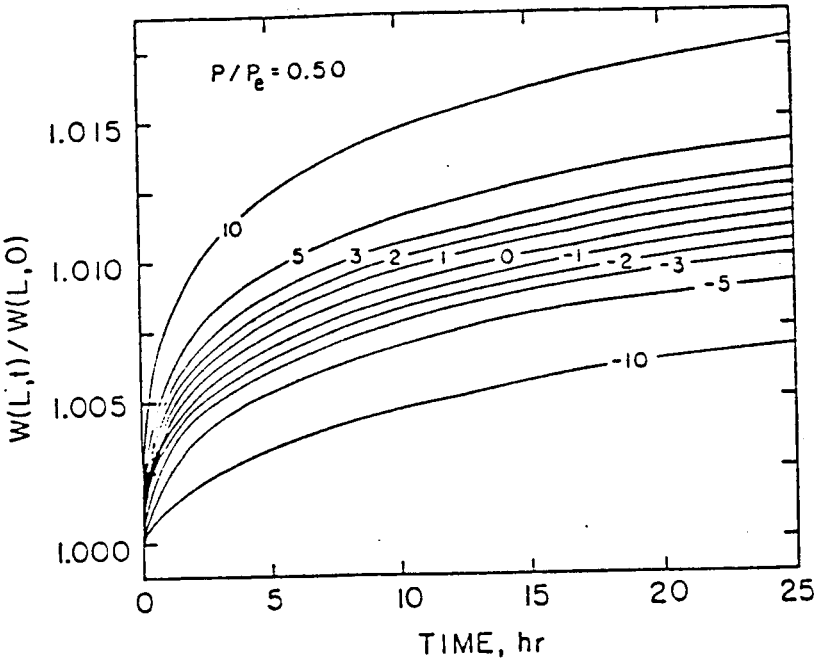

Figure 12 Influence of Temperature Differences on a 400 °C Beam-Column.

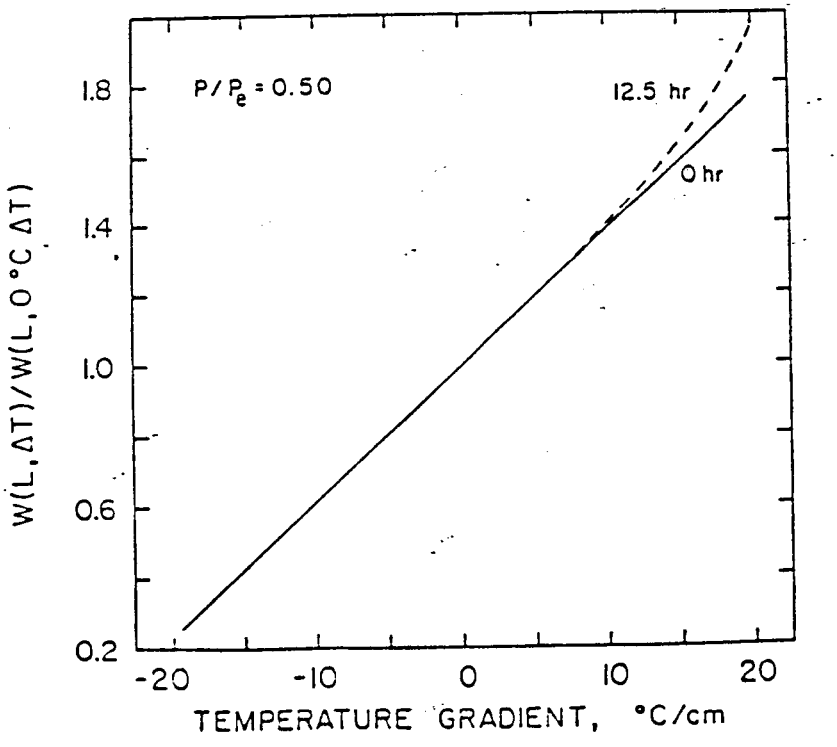

Figure 13 Transverse Deflection as a Function of Temperature Gradient at 600 °C.

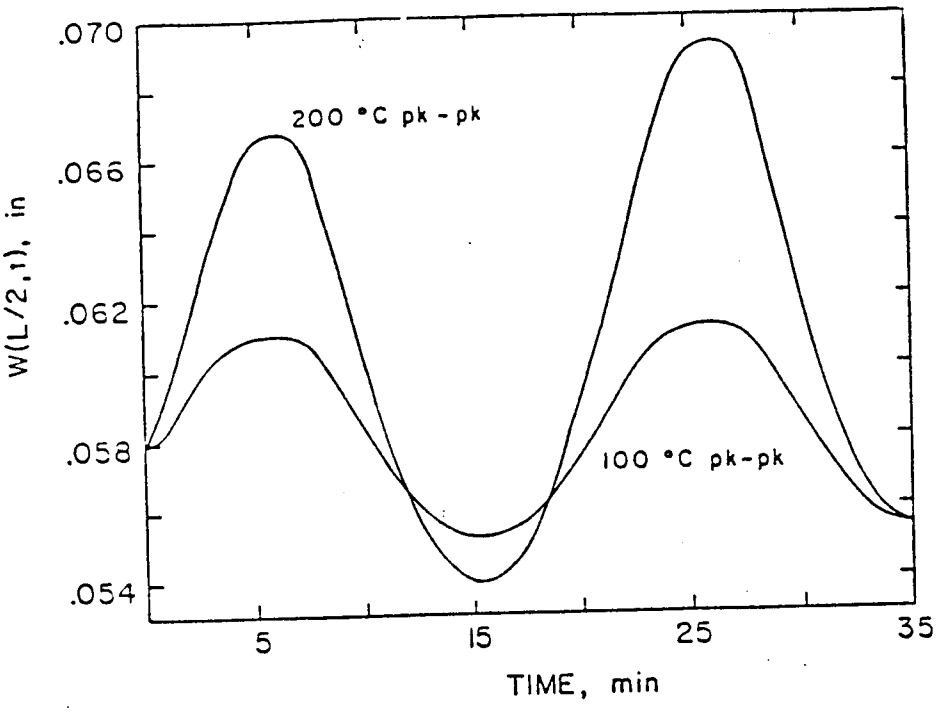

Figure 14 Low Arch Deflection for 50 and 100 °C Temperature Variations

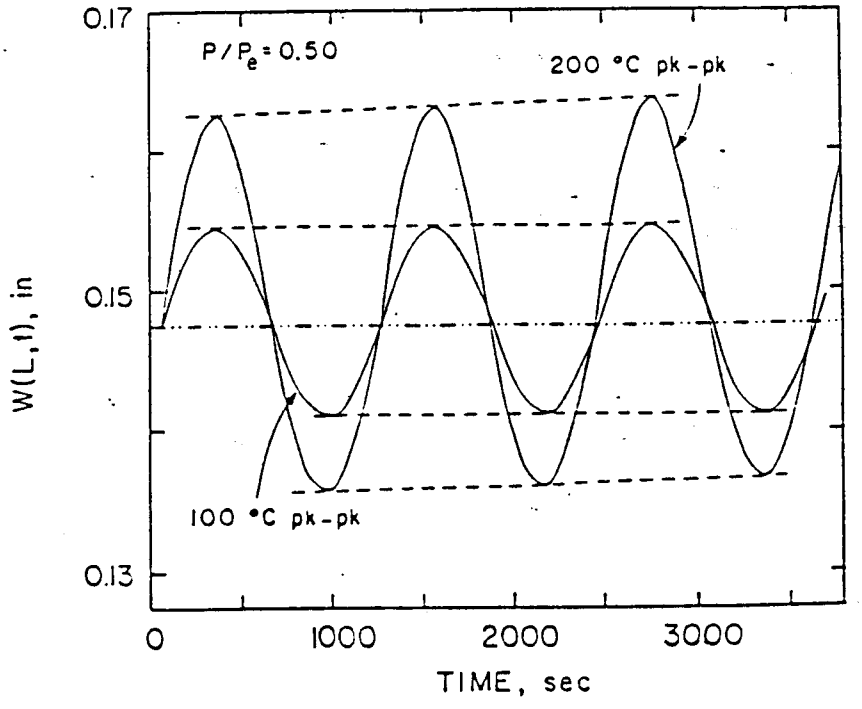

Figure 15 End Deflection for 50 and 100 °C Amplitude Temperature Variations

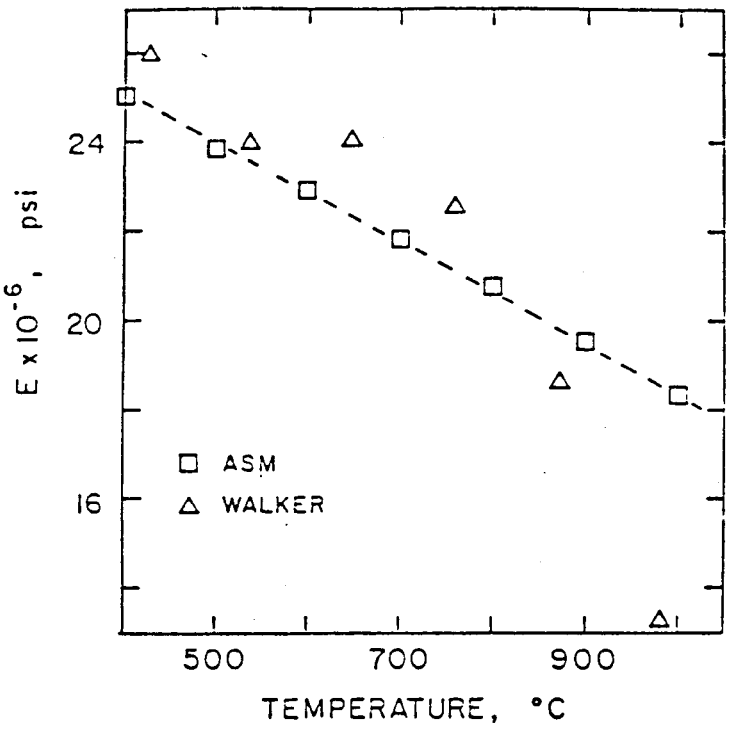

Figure A-1 Young's modulus as a Function of Temperature

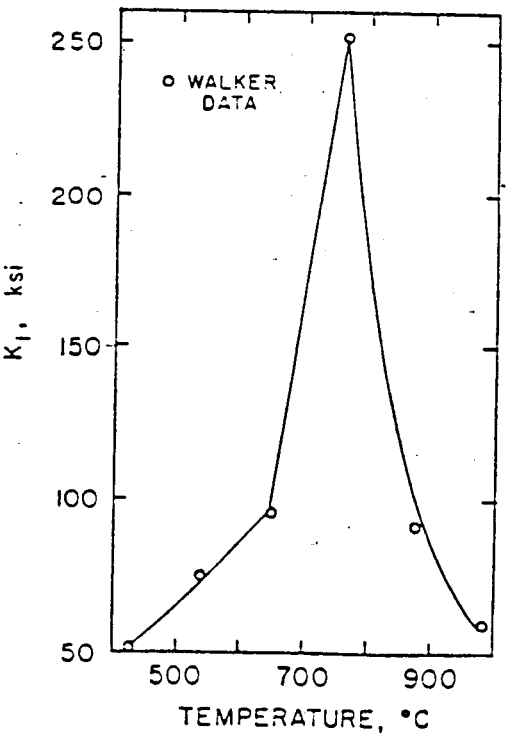

Figure A-2 K_I as a Function of Temperature

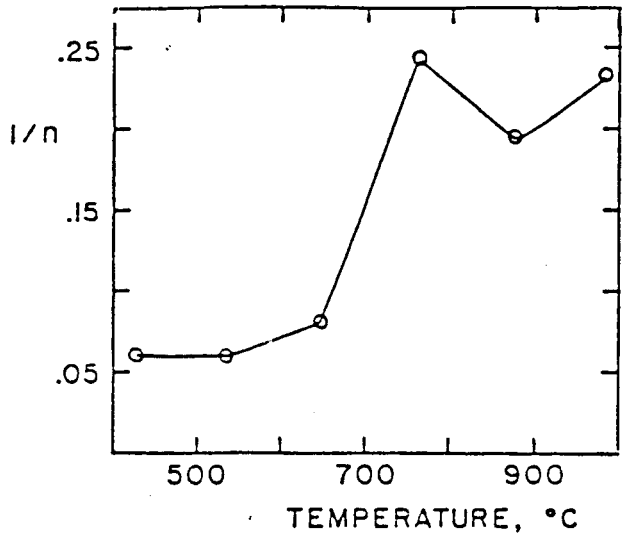

Figure A-3 n^{-1} as a Function of Temperature

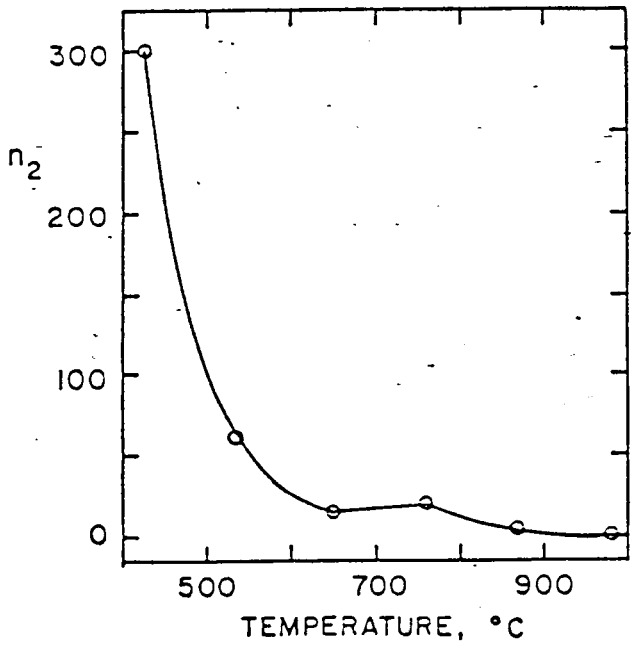

Figure A-4 n_2 as a Function of Temperature

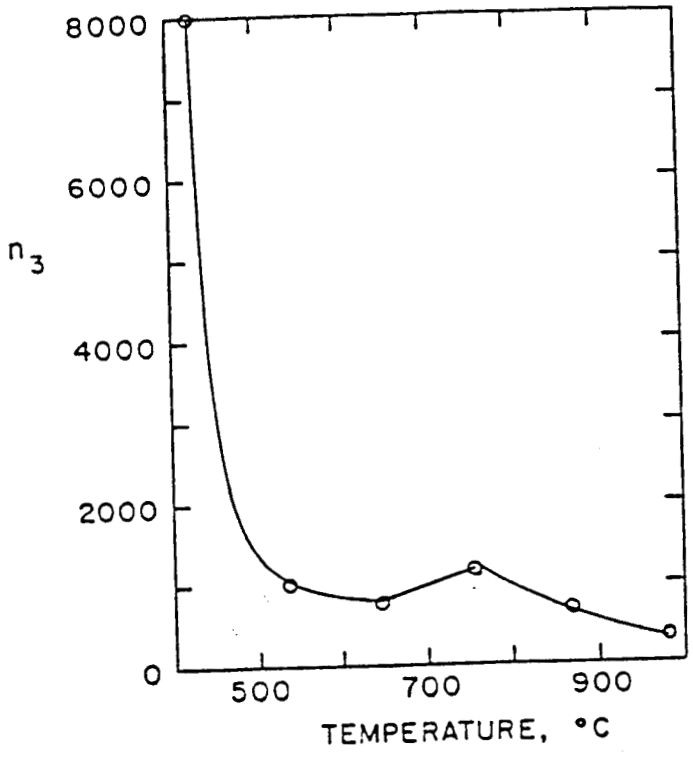

Figure A-5 n_3 as a Function of Temperature

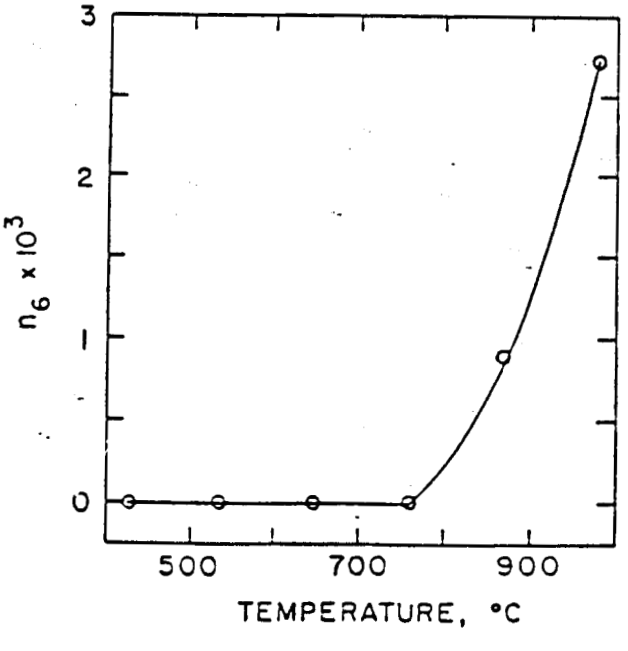

Figure A-6 n_6 as a Function of Temperature

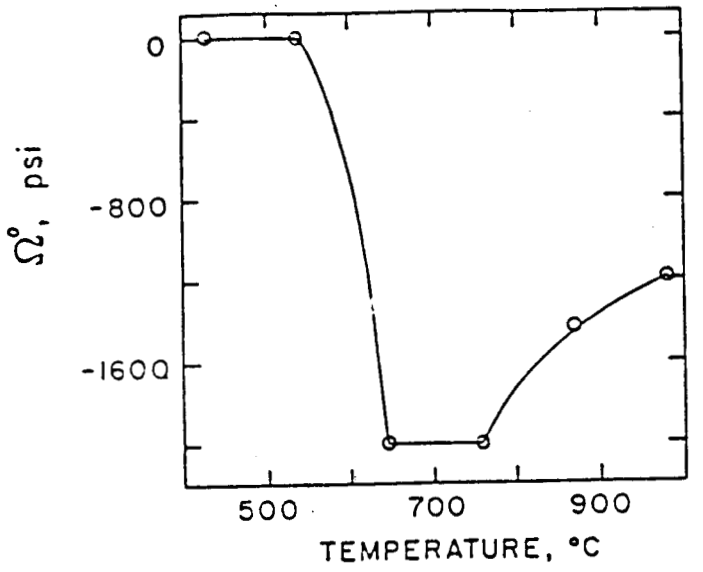

Figure A-7 Reference Backstress, Ω° as a Function of Temperature